TRANSPORTATION RESEARCH CENTER

# Air Convection Embankment Experimental Feature Design Phase I

by

Douglas J. Goering

December 1997

FINAL REPORT

Report No. INE/TRC 97.06
AK-RD-98-01
AKDOT&PF No. AK-RD-97-02

TRANSPORTATION & PUBLIC FACILITIES · STATE OF ALASKA

U.S. Department of Transportation
Federal Highway Administration

INSTITUTE OF NORTHERN ENGINEERING
INE
UAF RESEARCH CENTER

UNIVERSITY OF ALASKA FAIRBANKS
FAIRBANKS, ALASKA
99775-5900

# Technical Report Documentation Page

| 1. Report No.<br>INE/TRC 97.06 or AK-RD-97-02 | 2. Government Accession No. | 3. Recipient's Catalog No. |
|---|---|---|
| 4. Title and Subtitle<br>Air Convection Embankment Experimental Feature Design Phase I | | 5. Reporting Date<br><br>6. Performing Organization Code |
| 7. Author(s)<br>Douglas J. Goering | | 8. Performing Organization Report No.<br>INE/TRC 97.06 |
| 9. Performing Organization Name and Address<br>Institute of Northern Engineering<br>University of Alaska Fairbanks<br>Fairbanks, AK 99775-5900 | | 10. Work Unit No. (TRAIS)<br><br>11. Contract or Grant No. |
| 12. Sponsoring Agency Name and Address<br>State of Alaska<br>Alaska Dept. of Transportation and Public Facilities<br>Engineering and Operations Standards<br>3132 Channel Drive<br>Juneau, Alaska 99801-7898 | | 13. Type of Report and Period Covered.<br>Interim, 1996-97<br><br>14. Sponsoring Agency Code<br>SPR-95-08 |

15. Supplementary Notes

Performed in cooperation with the Federal Highway Administration.

16. Abstract

Prior research work (Goering and Kumar, 1996; and Goering, 1996) has indicated that Air Convection Embankments are a promising technique for limiting the thaw settlement damage that often occurs when roadway embankments are constructed in regions of warm permafrost. These studies lead to the proposal of a full-scale experimental Air Convection Embankment (ACE) to be constructed through the Federal Experimental Features in Construction Program. A work plan for including an ACE in the Parks/Chena Ridge Interchange project (Federal Project No. I-0A4-5(7), State of Alaska Project No. 63538) was forwarded and approved in 1994. This project report discusses the design and construction of the Parks/Chena Ridge ACE experimental feature which occurred during 1996 and 1997.

| 17. Key Words | | 18. Distribution Statement | |
|---|---|---|---|
| 19. Security Classif. (of this report)<br>nonclassified | 20. Security Classif. (of this page)<br>nonclassifed | 21. No. of Pages<br>73 | 22. Price |

# AIR CONVECTION EMBANKMENT ENVIRONMENTAL FEATURE DESIGN PHASE I

## FINAL REPORT

by

Douglas J. Goering
Associate Professor of Mechanical Engineering
University of Alaska Fairbanks
Fairbanks, Alaska 99775-5900

December 1997

Sponsored by

The Alaska Department of Transportation & Public Facilities
Statewide Research
2301 Peger Road
Fairbanks, Alaska 99709-5399

in cooperation with

the U.S. Department of Transportation
Federal Highway Administration

# DISCLAIMER

The contents of this report reflect the views of the author, who is responsible for the accuracy of the data presented herein. This research has been funded by the Alaska Department of Transportation and Public Facilities (ADOT&PF). The contents of the report do not necessarily reflect the views or policies of ADOT&PF or any local sponsor. This work does not constitute a standard, specification, or regulation.

# ABSTRACT

Prior research work (Goering and Kumar (1996), and Goering (1996)) has indicated that Air Convection Embankments are a promising technique for limiting thaw settlement damage that often occurs when roadway embankments are constructed in regions of warm permafrost. These studies lead to the proposal of a full-scale experimental Air Convection Embankment (ACE) to be constructed through the federal Experimental Features in Construction Program. A work plan for including an ACE in the Parks/Chena Ridge Interchange project (Federal Project No. I-0A4-5(7), State of Alaska Project No. 63538) was forwarded and approved in 1994. This project report discusses the design and construction of the Parks/Chena Ridge ACE experimental feature which occurred during 1996 and 1997.

# TABLE OF CONTENTS

LIST OF FIGURES

# LIST OF TABLES

# ACKNOWLEDGMENT

Funding for this research was provided by the Alaska Department of Transportation and Public Facilities under project SPR-UAF-95-08, "Air Convection Embankment Experimental Feature Design." Additional support has been provided by the Alaska Science and Technology Foundation under grant #92-2-1110, "Enhanced Convection for Roadway Stabilization." The author would also like to acknowledge the support of the Arctic Region Supercomputer Center at the University of Alaska Fairbanks through a grant for computing resources.

# 1.0 INTRODUCTION

The Air Convection Embankment (ACE) has been the focus of two previous studies conducted by the author and funded by the Alaska Department of Transportation and Public Facilities (ADOT&PF) and the Alaska Science and Technology Foundation (ASTF). Results from the ADOT&PF study have been summarized in Goering and Kumar (1996). This paper contains a description of the ACE concept and a summary of a modeling study which was carried out to investigate the thermal performance of these embankments. Briefly, the ACE concept involves the use of a highly porous, poorly graded embankment material, such as gravel or rock with a low fines content, which is used to construct the main portion of the embankment. Such a material allows convection of the pore air to occur within the embankment. During winter months the asphalt surface of the embankment will be maintained at very low temperatures due to low atmospheric air temperatures and snow removal. This situation results in very low temperatures in the upper portion of the embankment, while the lower portions of the embankment and underlying foundation materials remain relatively warm. The result is an unstable air density gradient within the embankment during typical winter-time conditions. With a porous embankment material of sufficient air permeability, this unstable density gradient will result in circulation of the pore air and enhanced winter time heat transfer. During summer months the embankment air density gradients are stable and circulation will not occur. Thus the embankment acts as a sort of one-way heat transfer device or thermal diode which effectively removes heat from the embankment and underlying foundation material during winter months without re-injecting heat during subsequent summers.

Modeling results and data from a pilot experimental study have indicated that the operational scenario discussed above is substantially accurate, (Goering, 1996). The results showed complicated patterns of natural convection within the embankment during winter months which resulted in a significantly enhanced cooling of the embankment foundation. The results also showed that the pore-air was practically stagnant during summer months and did not enhance summer heat transfer. Overall the numerical results predicted a net lowering of mean annual temperatures at the base of the embankment which ranged from 7-10°F (3.9-5.6°C) when compared to a standard sand/gravel (non-ACE) embankment. This result was subsequently confirmed by data collected from a pilot ACE embankment which was constructed at Brown's Hill Quarry near Fairbanks, AK. Yearly average temperatures obtained during two years of operation of this embankment indicated mean annual temperatures that ranged from 33-36°F (1-2.2°C) near the upper surface of the embankment to 25-29°F (-3.9 to -1.7°C) at its base.

In order to move the ACE concept toward practical application in Alaska, an Experimental Feature in Construction was approved for inclusion in the Parks/Chena Ridge Interchange Project which is currently in the final stages of construction. This report describes the planning and design activities associated with this experimental feature. The original project, which was funded by ADOT&PF in 1995, included only planning and design activities. The project has recently been extended to also include three years of monitoring activity. As a consequence, the project has now been subdivided into Phase 1 and Phase 2. Phase 1 included the planning and design

activities which are now complete. The specific tasks associated with the Phase 1 portion of the project (as outlined in the original proposal) include:

- Basic ACE test section configuration established, including cross-sectional geometry, material requirements, side-slope conditions, and pavement structure requirements.
- Completion of modeling studies aimed at investigating the proposed geometry, side-slope treatment and pavement structure.
- Consultation with ADOT&PF personnel regarding proposed ACE design. Consultation with instrumentation subcontractor to facilitate sensor construction and data logging equipment installation.
- Testing of material proposed for use in construction of the ACE test section and consulting with contractor/ADOT&PF concerning suitability of proposed material.
- Connection and programming of data logging system and collection of initial temperature data.
- Report preparation and presentation.

Originally it was anticipated that construction would be completed during the summer of 1996, and the original end date for the (Phase 1) project was September of 1996. However, the construction of the ACE test section did not commence until September 15 of 1996 and the completion date for the Phase 1 work was extended until the spring of 1997.

The remainder of this report discusses the project tasks outlined above.

# 2.0 ACE TEST SECTION CONFIGURATION

During the spring of 1995 several meetings were held with Bob McHattie, Nancy Burkholtz, Joe Keeny, and Malcom Pearson of the Northern Region AKDOT&PF office in an effort to establish an appropriate ACE test section configuration. Bob McHattie was instrumental early on in terms of identifying an appropriate project and site for the ACE Experimental Feature. The idea was to find a location with a thaw-unstable permafrost foundation that had not been disturbed by previous building projects. The Parks/Chena Ridge Interchange project contains a new segment of road that meets these requirements. In particular Bob McHattie was able to identify a section of that project stretching from station 706 to 709 that was appropriate for both a test and control section. It was desired to include the control section in addition to the actual ACE test section in order to have benchmark data for the non-ACE roadway. This data is to be used to evaluate the cooling effectiveness of the ACE section as compared to the standard road section. Since the project was already well into the planning stages at that point, much of the embankment configuration (size, shape, width, height, etc.) had already been determined. Our discussions centered on how to modify the existing plans to include the ACE test section and a control section.

## 2.1 Test Section

Specification of the test section configuration required us to address embankment geometry, material requirements, construction details, and instrumentation requirements. It was decided to include a 200 ft (61 m) ACE test section stretching

from station 707 to 709. The shape of the embankment in this area was to be unaltered from the original plans, however, the embankment material was specified as a large open graded aggregate, conforming to the gradation specification given in Table 1. Examination of Table 1 reveals that the material consists, essentially, of cobbles in the 3"-6" (7.6 - 15.2 cm) size range. In addition to the ACE material, it was also necessary to alter the original plans by removing the 4" (10.2 cm) of insulation board from the embankment in this area. In order to provide for the pavement structure, the ACE material was to be covered with a geotextile separator and then topped with well-graded material prior to placement of the asphalt pavement. The side slope in the 1:6 region of the barn roof embankment was to be covered with a choke layer placed over the top of the ACE material in order to provide a smoother surface. In the 1:1.5 region, the side slope was to be left with the ACE material directly exposed to the ambient air. Figure 1. (taken from the construction plans) shows the resulting ACE cross section.

Table 1. ACE Material Gradation

| Sieve Size | Cumulative % Passing |
|---|---|
| 6" (15.2 cm) | 100 % |
| 4" (10.2 cm) | 5 - 100 % |
| 3" (7.6 cm) | 0 - 5 % |
| 1" (2.5 cm) | 0 - 3 % |
| #10 | 0 - 2 % |

In addition to the mechanical configuration of the embankment, it was also necessary to design a complete instrumentation system capable of accurately characterizing the thermal behavior of the ACE test section. This was accomplished by specifying the

inclusion of an array of thermistor temperature sensors located on 2 × 2 ft (61 × 61 cm) centers throughout the center plane of the test section (at station 708). This resulted in a total of 5 separate thermistor strings and 140 thermistor sensors located within the ACE embankment cross section. In addition, three vertical strings (with an additional 18 thermistor sensors) were drilled into the foundation material at station 708 in order to assess temperatures beneath the ACE test section. The positions of the eight thermistor strings (labeled D, E, F, G, H, I, J, and K) are shown in Figure 1. Each of these thermistor strings was armored with schedule 80 PVC electrical conduit with aluminum rings placed over each sensor. A Campbell Scientific data logging system which included a processor module, 5 signal multiplexers, and two storage modules was specified for use with the thermistor strings. The data logging system was to be housed in a highway traffic controller box to be located adjacent to the ACE test section at station 708 as shown in Figure 1. A complete description of the thermistor strings, data logging system, and wiring diagrams can be found in the construction plans for the Parks/Chena Ridge Interchange Project (see references).

## 2.2 Control Section

Figure 2 (also taken directly from the construction plans) shows the control section which is located at station 706. The mechanical design of the embankment at the control section was unaltered from the original plans, with the exception of the inclusion of instrumentation. Figure 2 shows the location of the insulation board and thermistor sensor strings (labeled A, B, and C) with respect to the surface of the embankment. Strings A and B contain 10 thermistor sensors each, the uppermost of

which is located immediately above the insulation board. String C contains 8 sensors. Thermistor cables from the control section are routed to a pedestal-mounted multiplexer box (Figure 2.) and then to the main controller box at station 708.

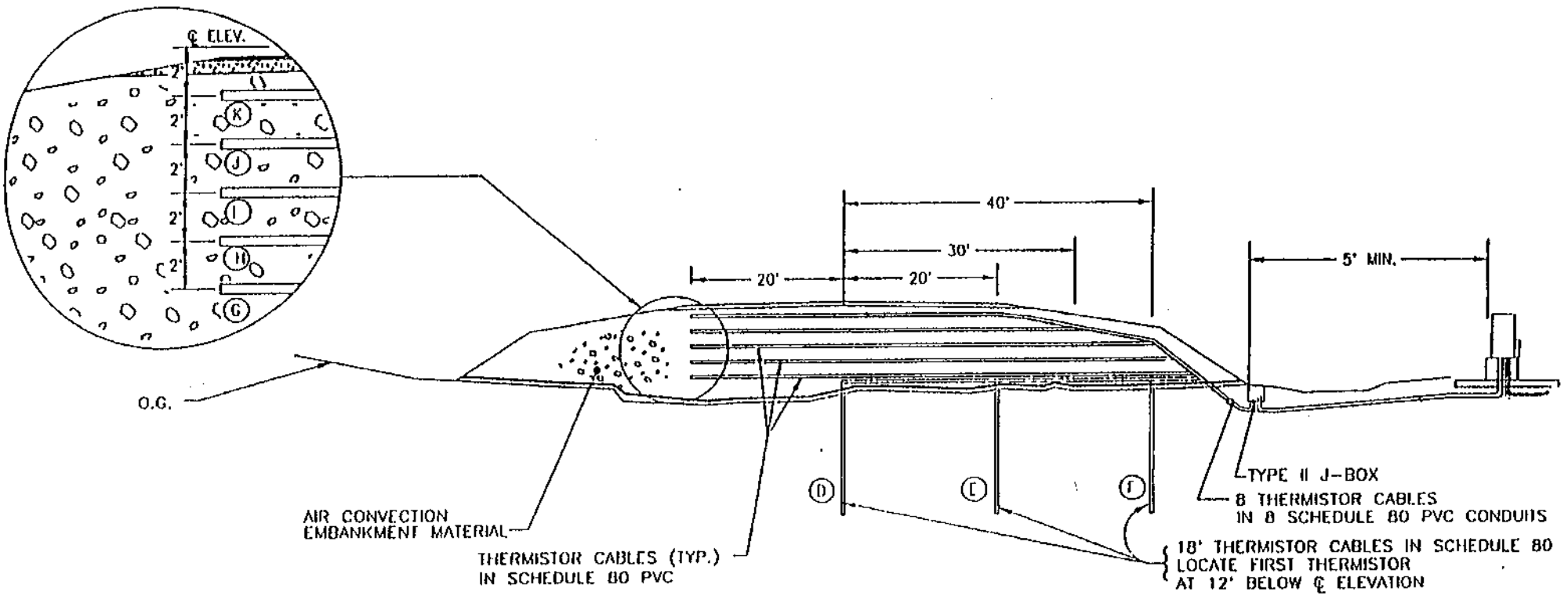


Figure 1. ACE test section configuration.

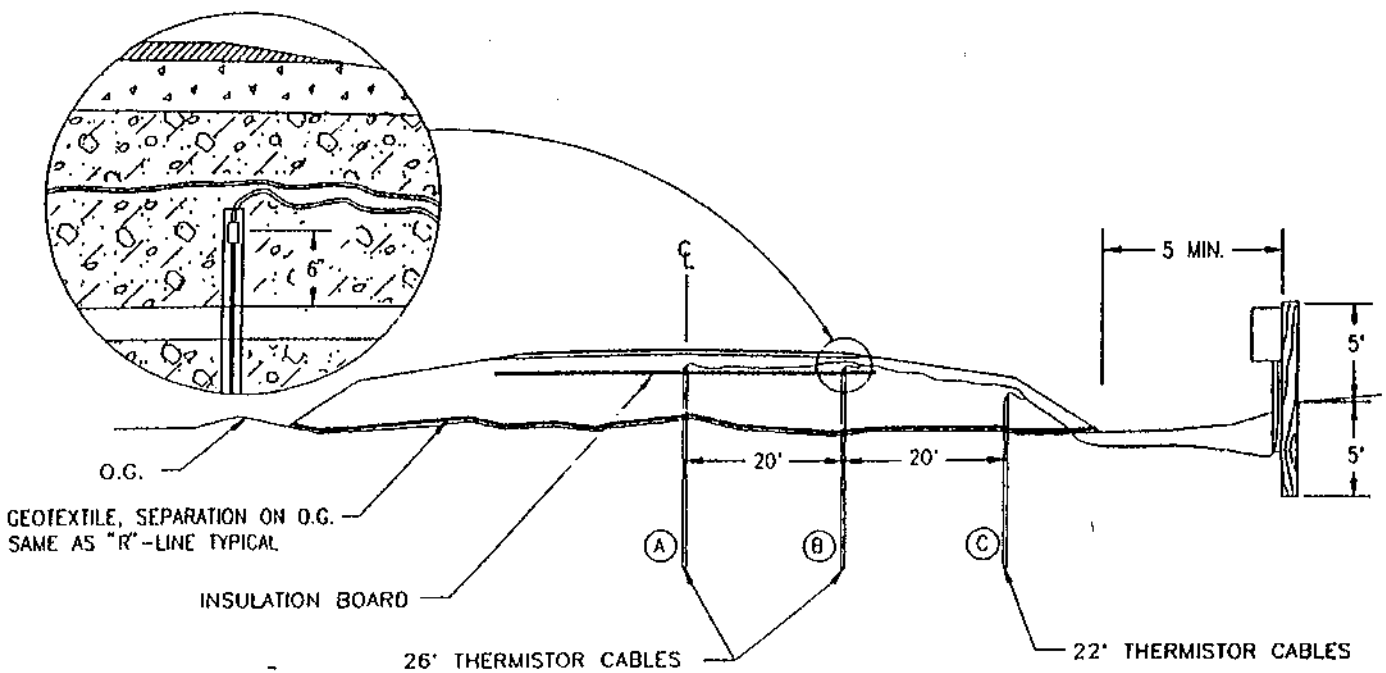


Figure 2. Control section configuration.

# 3.0 MODELING STUDIES

## 3.1 Background

During the spring and summer of 1996, modeling studies aimed at investigating the effectiveness of the Parks/Chena Ridge ACE Experimental Feature were completed. There were two areas of primary concern which were addressed by the modeling studies. These included the effect of the relatively impermeable pavement structure and the effect of the open side-slope boundary on the operation of the embankment. It was suspected that the pavement structure (including a geotextile separator, crushed aggregate base course (hereafter referred to as the D-1 layer), and asphalt layer) would have a detrimental impact on ACE operation. This follows from the fact that this highly-compacted layer has a low air permeability and, therefore reduces the strength of the natural convection. The effect of an open side-slope boundary was expected to be beneficial since it allows cold ambient air to penetrate into the embankment structure. This phenomena was noted during the operation of a test embankment at Brown's Hill Quarry during the 1993-1995 time frame. Low temperature ambient air was observed to enter the toe of the embankment side slope through the snow layer during winter months and exit out the upper portion of the side slope. As a consequence, enhanced cooling was achieved in the side-slope region.

In order to assess the effects of these two features, a series of three numerical simulations were carried out. All three made use of the proposed Parks/Chena Ridge

embankment geometry as shown in Figure 1 and temperature boundary conditions which are representative of the Fairbanks area. The first of the simulations is referred to as the Base Case and consisted of an embankment with an asphalt layer, compacted D-1 layer, and open side slopes. The Base Case corresponds to the Parks/Chena Ridge ACE configuration as proposed and described in the previous section. In order to investigate the effect of the pavement structure, an additional 3-Layer Case was run in which the D-1 layer was replaced with high-permeability rock. Finally, in order to investigate the effect of the open side-slope boundary, a Closed Side-Slope Case was run in which the side-slope boundary was considered to be impermeable (such would be the case if, for instance, the side slopes were covered with a layer of geotextile and top soil).

The numerical simulations were carried out with the aid of a two-dimensional unsteady finite element model described previously by Goering and Kumar (1994). Briefly, this model solves the unsteady momentum and energy equations assuming Darcy flow and making used of the Bousinesq approximation to include the effects of buoyancy. Simulations were carried out on the Arctic Region Supercomputing Center's Cray YM-P and on Unix workstations within the Mechanical Engineering Department at UAF. Modifications of the previous model were required in order to include the effect of the open side-slope boundaries. A discussion of these modifications along with a comprehensive description of the simulations which were carried out for the three cases described above can be found in Tu (1996).

Figure 3 shows the layer geometry which was used in the numerical model. Both the Base Case and the Closed Side-Slope Case used the four layers as shown in the figure. For the 3-Layer Case, the sandy gravel (D-1) layer was replaced with rock. The material properties used for each of the four layers are listed in Table 2.

Table 2. Material Properties.

| Layer | Property | Value |
|---|---|---|
| Layer 1, Asphalt: | Thermal conductivity | 0.42 Btu/hr ft °F (0.73 W/m°C) |
| | Specific Heat | 27 Btu/ft$^3$°F (1811 kJ/m$^3$°C) |
| | Latent Heat | 0 |
| | Permeability | 0 |
| Layer 2, D-1: | Thawed thermal conductivity | 1.5 Btu/hr ft °F (2.6 W/m°C) |
| | Frozen thermal conductivity | 1.4 Btu/hr ft °F (2.43 W/m°C) |
| | Thawed specific Heat | 29.7 Btu/ft$^3$°F (1992 kJ/m$^3$°C) |
| | Frozen specific Heat | 27 Btu/ft$^3$°F (1811 kJ/m$^3$°C) |
| | Latent Heat | 777.6 Btu/ft$^3$ ($2.9\times10^4$ kJ/m$^3$) |
| | Permeability | 0 |
| Layer 3, ACE Rock: | Thermal conductivity | 0.2 Btu/hr ft °F (0.35 W/m°C) |
| | Specific heat | 15 Btu/ft$^3$°F (1006 kJ/m$^3$°C) |
| | Latent heat | 0 |
| | Permeability | $6.8\times10^{-6}$ ft$^2$ ($6.32\times10^{-7}$ m$^2$) |
| Layer 4, Silty Soil: | Thawed thermal conductivity | 0.86 Btu/hr ft °F (1.49 W/m°C) |
| | Frozen thermal conductivity | 1.34 Btu/hr ft °F (2.32 W/m°C) |
| | Thawed specific Heat | 55.8 Btu/ft$^3$°F (3742 kJ/m$^3$°C) |
| | Frozen specific Heat | 35.5 Btu/ft$^3$°F (2381 kJ/m$^3$°C) |
| | Latent Heat | 5832 Btu/ft$^3$ ($2.17\times10^5$ kJ/m$^3$) |
| | Permeabilty | 0 |

In addition to material properties, it was also necessary to specify appropriate boundary conditions at the ground surface. These included three separate harmonic temperature functions for the gravel side slope, native ground surface (vegetated surface), and for the pavement surface. In each case the temperature functions were

derived based on air temperature data for the Fairbanks area which indicates a mean annual air temperature of 26°F (-3.3°C), an air thawing index of 3000 °F-days (1667 °C-days) and an air freezing index of 5500 °F-days (3055 °C-days). Separate freeze and thaw n-factors were use to generate the final harmonic temperature functions. The resulting temperature functions (with t in days from January 1) and n-factors are listed in Table 3 for each of the three surface types.

Table 3. Temperature Boundary Conditions.

| Surface | Thaw n-factor | Freeze n-factor | Temperature function |
|---|---|---|---|
| Pavement | 1.9 | 0.9 | 34-46.9cos[2π/365(t-9)] °F<br>1.1-26.1cos[2π/365(t-9)] °C |
| Gravel side slope | 1.7 | 0.6 | 36.9-37.6cos[2π/365(t-9)] °F<br>2.7-20.9cos[2π/365(t-9)] °C |
| Native surface | 0.5 | 0.5 | 28.5-18cos[2π/365(t-9)] °F<br>-1.9-10cos[2π/365(t-9)] °C |

The simulations were carried out using a finite element grid which contained 3333 nodes and 6400 elements. The actual grid geometry is shown in Figure 4.

## 3.2 Base Case.

The first simulation which was carried out, referred to as the Base Case, included an embankment with the geometry corresponding to that shown in Figure 3. All four layers were used, silt soil foundation, ACE rock, compacted sand/gravel (D-1), and asphalt. In this case the side slope of the embankment was left open. This configuration corresponds to the Parks/Chena Ridge ACE embankment design as it

was originally proposed (and eventually built). Figures 5(a)-(f) show plots of isotherms and velocity vectors which were obtained for the Base Case simulation on May 31, July 30, September 28, November 27, January 1, and March 2. In these plots temperature isotherms are shown on the left-hand side with the corresponding velocity vector field shown on the right.

Figures 5(a) and (b) are typical of summer conditions. In both cases the isotherms are relatively flat and horizontal. This suggests that any convection which may be occurring during the summer months is weak and does not have a significant effect on the temperature within the embankment. Both of these figures indicate that the ground temperatures are relatively low beneath the embankment in comparison with the adjacent undisturbed soils. Figure 5(c) shows that the convection is beginning to have a significant effect on the temperatures within the embankment by the end of September. In this case the isotherms are beginning to depart from the relatively straight horizontal form that they display during the summer months. By the end of November, the convection has increased in strength to the point where it is the primary controller of temperature profiles in the embankment. This can be seen in Figure 5(d), which shows that the temperature and flow patterns are closely related. This type of behavior persists throughout the winter months (stretching from November-March). The convection cells apparent in Figures 5(d), (e), and (f) have a large cooling influence on the lower portion of the embankment and subgrade. The cells are still very strong in January but begin to reduce in intensity during March (see Figures 5(e) and (f)).

Figures 6, 7, and 8 show the yearly minimum, maximum and average temperatures within the embankment and foundation. Figure 6 shows that the minimum temperatures within the embankment itself are dominated by the shape of the convection cells displayed in Figures 5(d)-(f). Note that, in general, the foundation soils are colder beneath the embankment than they are in the surrounding undisturbed areas. Figure 7 shows the maximum temperatures which are reached during the annual cycle. This particularly important since it displays the maximum depth of thaw. The figure shows that the freezing isotherm does not move down as deeply into the foundation soils beneath the embankment as it does in the adjacent soils. What this shows is that the permafrost table has actually agraded beneath the embankment and the roadway should, therefore, be free of problems caused by melting pre-existing permafrost. Finally, Figure 8 shows the mean annual temperature of the embankment and foundation soil. It tends to indicate lower average temperatures in the lower portion of the embankment and foundation soil. Note that the upper portions of the embankment experience relatively high mean temperatures. This is a direct result of unfavorable thermal conditions which produce very high summer temperatures at the embankment surfaces. Other conditions which tend to produce high summer temperatures (such as concentration of surface water flow at the embankment toes) have not been included in the present study.

## 3.3 3-Layer Case.

The second simulation which was carried out attempted to quantify the detrimental effect of the pavement structure. This effect is due primarily to the presence of a low

permeability supporting layer of compacted material immediately beneath the asphalt. This layer will inhibit the natural convection to some extent by reducing the overall height of the convecting layer (essentially reducing the height of the "chimney"). The effect of this layer was assessed by running the 3-Layer Case with the pavement support layer (layer 2 shown in Figure 3) removed from the model and replaced with ACE rock. This simulation only included 3 layers; silt foundation soil, ACE rock, and asphalt.

Figures 9(a)-(f) show plots of the temperature isotherms and velocity vectors for dates of June 2, August 2, October 2, December 2, January 1, and March 3. In general, seasonal trends are similar for the 3-Layer and Base Cases. Convection occurs during the winter months but not during the summer. Examination of Figures 9 (e), (d), and (f) indicates that the convection which occurs in the roadway embankment during winter months is dominated by a single pair of large circulation cells centered beneath each driving lane. These cells provide a large amount of winter cooling and lower the temperature of the foundation soil beneath the driving lanes. Figure 9(e) shows that the lowest foundation temperatures are reached beneath the cold plume formed by these two cells.

Figures 10, 11, and 12 show the yearly minimum, maximum and average temperatures within the embankment and foundation for the 3-Layer Case. Trends are again similar to what was observed with the Base Case. The minimum temperature contours are dominated by the strong winter convection, and the influence of the two cells which exist beneath each driving lane is apparent in Figure 10. Maximum temperatures are

determined by summer-time conditions when convection is not active. The effect of this can be observed in Figure 11 which shows that maximum temperatures within the embankment have flat and horizontal contours and are not influenced by the shape of the convection cells. Figure 11 also shows that the permafrost table has agraded beneath the embankment, eliminating settlement due to thaw consolidation. Finally, Figure 12 shows mean annual temperatures for the 3-Layer Case. The effect of the two cells beneath each driving lane can again be observed in this figure. Note that the lowest mean temperatures are immediately beneath the driving lanes in the foundation soil.

### 3.4 Closed Side-Slope Case.

The purpose of the final simulation was to examine the impact of the side-slope boundary condition. This boundary can have a large impact on the thermal regime in the toe and side-slope region of the embankment. If the side-slope boundary is left open, as in the Base Case, ambient air can enter at the toe and move through the embankment providing additional cooling of this region during winter months. A closed side-slope implies that an impermeable barrier (such as a layer of top soil or a plastic covering) has effectively sealed the side-slope of the embankment, preventing any infiltration of ambient air. While this may have detrimental effects during the winter months when infiltrating air provides cooling, it likely would have a beneficial effect during summer when warm air would otherwise warm the toe region.

Figures 13(a)-(f) show plots of the temperature isotherms and velocity vectors for dates of June 2, August 2, October 2, December 2, January 1, and March 2. Again, in general, seasonal trends are similar to the 3-Layer and Base Cases. Convection occurs during the winter months but not during the summer. Examination of Figures 13 (e), (d), and (f) shows that patterns of winter-time convection are similar to the Base Case shown in Figure 5, with several pairs of circulation cells spaced out across the embankment. In this case, however, the pattern of circulation cells extends all the way to the toe of the embankment due to the lack of infiltration and exfiltration in the toe region.

Figures 14, 15, and 16 show the yearly minimum, maximum and average temperatures within the embankment and foundation for the Closed Side-Slope Case. The minimum temperature contours shown in Figure 14 are again dominated by the shape of the winter convection cells, while the maximum temperature profiles shown in Figure 15 are flat and horizontal. Figure 15 shows that this configuration also provides good permafrost protection with a maximum thaw depth that is more shallow beneath the embankment than it is beneath the undisturbed surface. Finally, Figure 16 shows that the mean annual temperatures are approximately the same beneath the embankment as they are beneath the undisturbed surface.

## 3.5 Comparison

Figure 8 shows mean annual temperature contours for the Base Case. From this figure it is apparent that the Base Case configuration is effective at lowering mean

temperatures beneath the embankment. A large area immediately beneath the embankment has a mean temperature which is lower than 26°F (-3.3°C). Figure 12 shows mean annual temperatures for the 3-Layer Case. As expected, the 3-Layer Case shows an improved cooling due to the lack of the convection restriction in the pavement structure layer (D-1 layer). Mean temperatures are about 2-3°F (1.1-1.6°C) colder beneath the embankment than those for the Base Case. Figure 16 shows mean annual temperatures for the Closed Side-Slope Case. This figure shows that the closed side-slope does have a significant detrimental effect on embankment operation with mean temperatures beneath the embankment that are approximately 1.5-2°F (0.8-1.1°C) warmer than those for the Base Case.

From the data shown in the figures, we can conclude that the embankment operation would be enhanced by leaving the side-slope boundary open and eliminating (or limiting the thickness of) the D-1 layer. The final design for the Parks/Chena Ridge ACE Experimental Feature does incorporate the use of an open side-slope boundary, although it is possible that the side-slope surface will eventually become covered with debris and act as a closed surface. The AKDOT&PF design staff was not comfortable with the idea of completely eliminating the D-1 layer (and paving directly on the rock) so, instead, it was agreed to limit the thickness of the D-1 layer to six inches in order to minimize its detrimental effect. The final construction actually consisted of a layer of choke rock (approximately ¾ inch (2 cm) aggregate) that was approximately 2 inches (5 cm) thick placed directly on top of the rock ACE layer. The choke layer was then covered with a treated base and pavement. The resulting pavement structure had a thickness of approximately 6-8 inches (15-20 cm) including the asphalt layer.

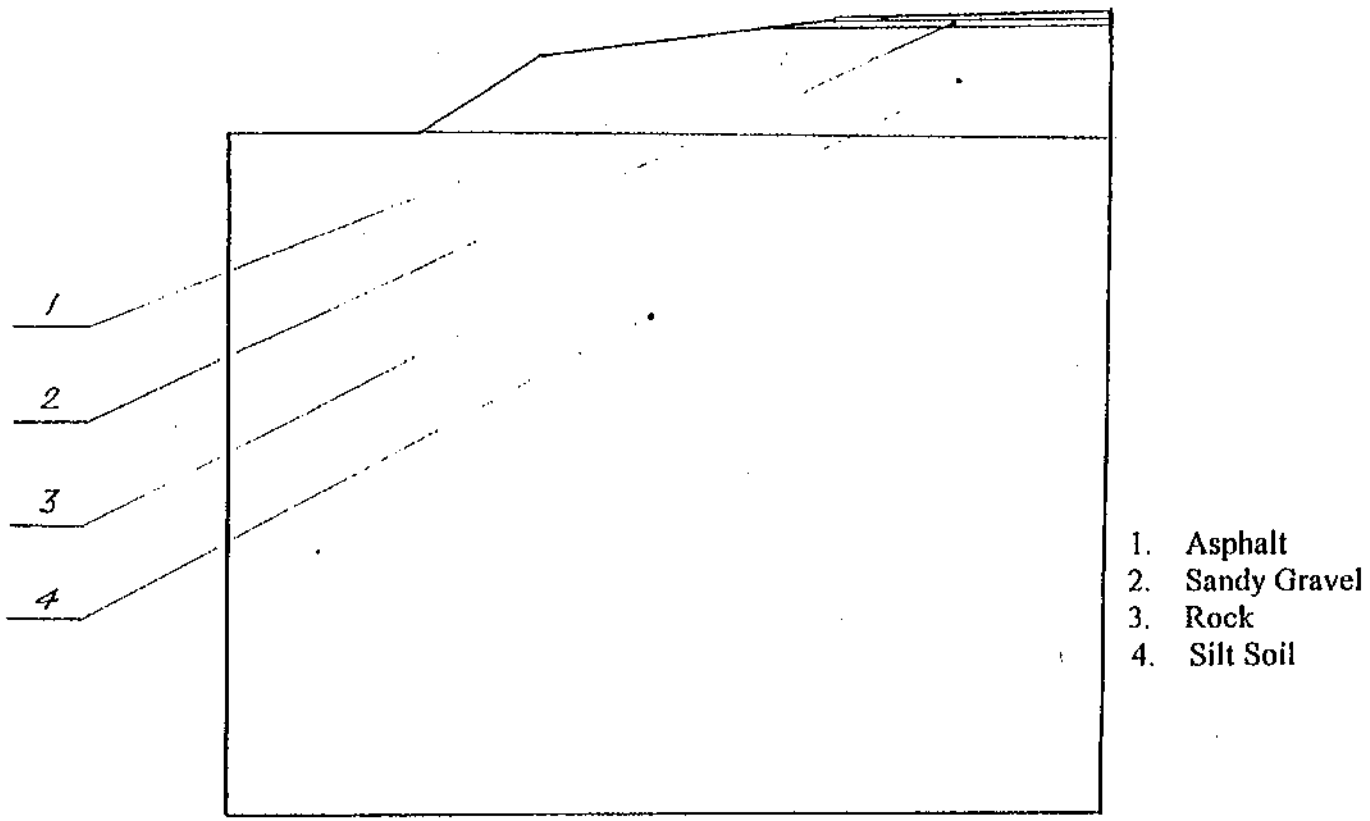


Figure 3. Model geometry employed for embankment simulations.

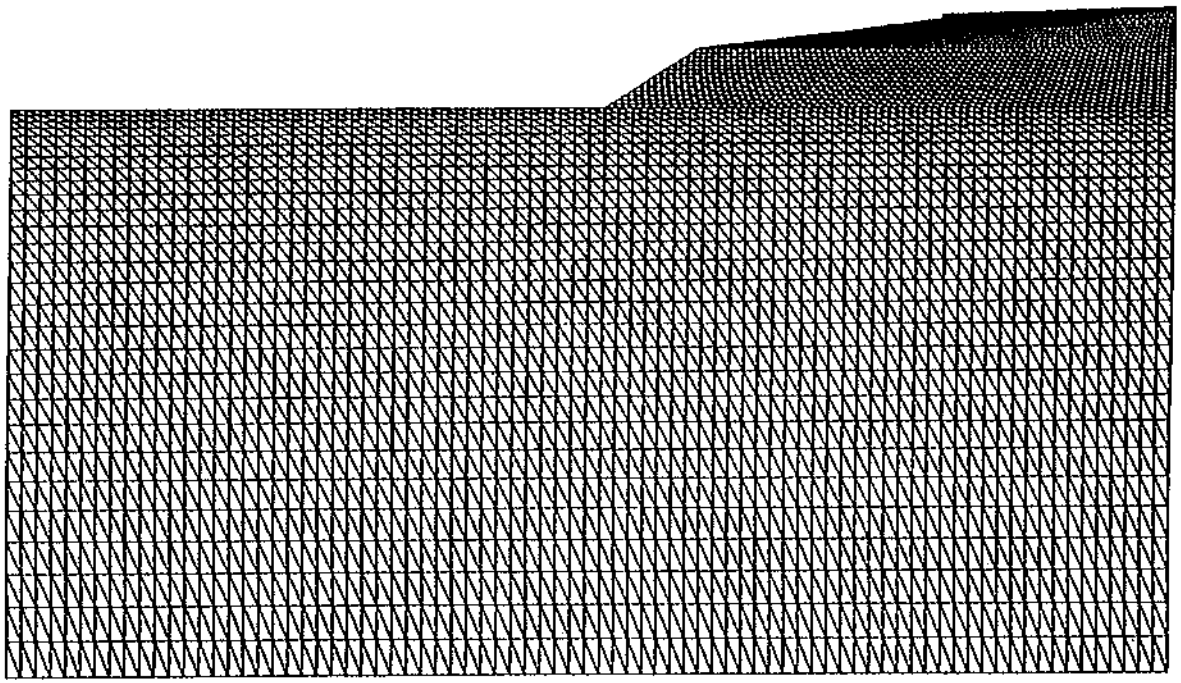

Figure 4. Finite element grid consisting of 3333 nodes and 6400 elements used for numerical simulations.

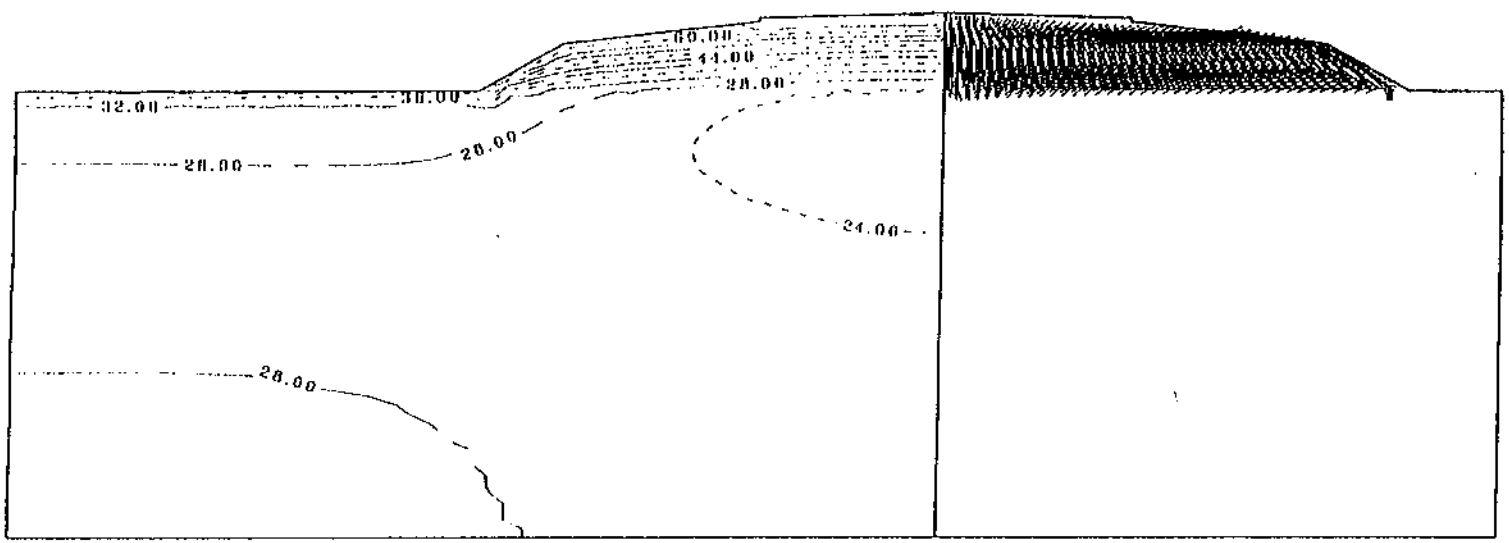


Figure 5(a). Isotherms (°F) and velocity vectors for the Base Case Simulation on May 31.

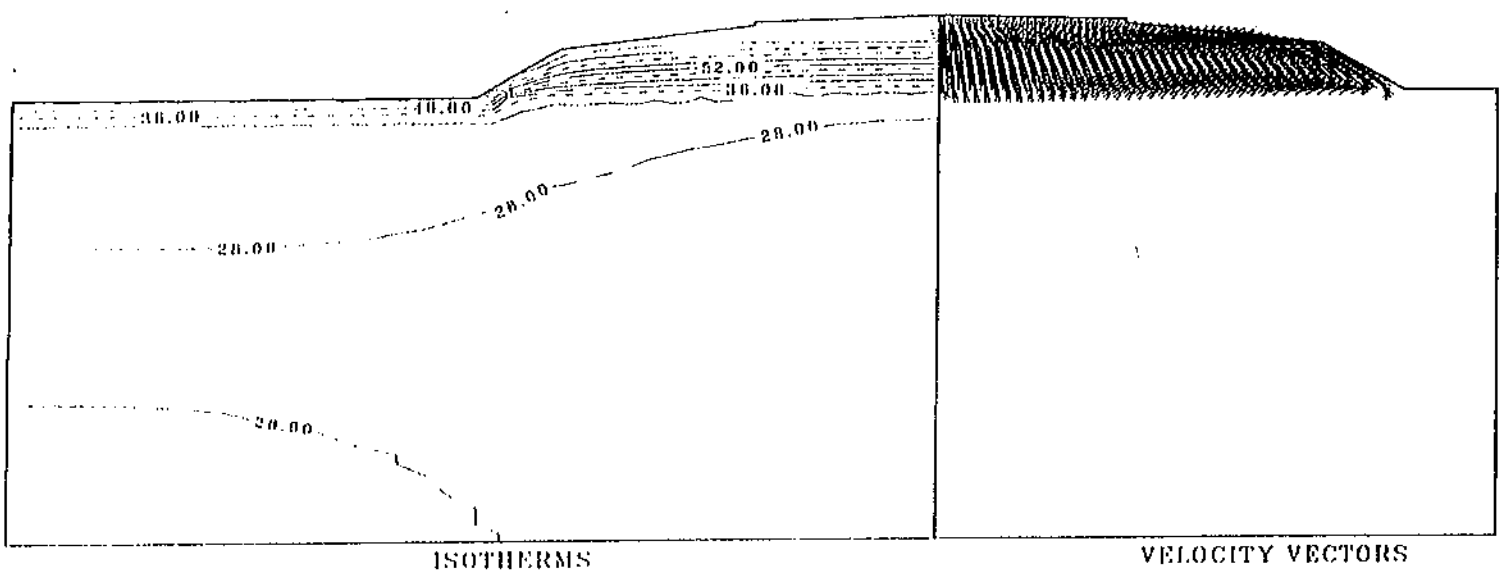


Figure 5(b). Isotherms (°F) and velocity vectors for the Base Case Simulation on July 30.

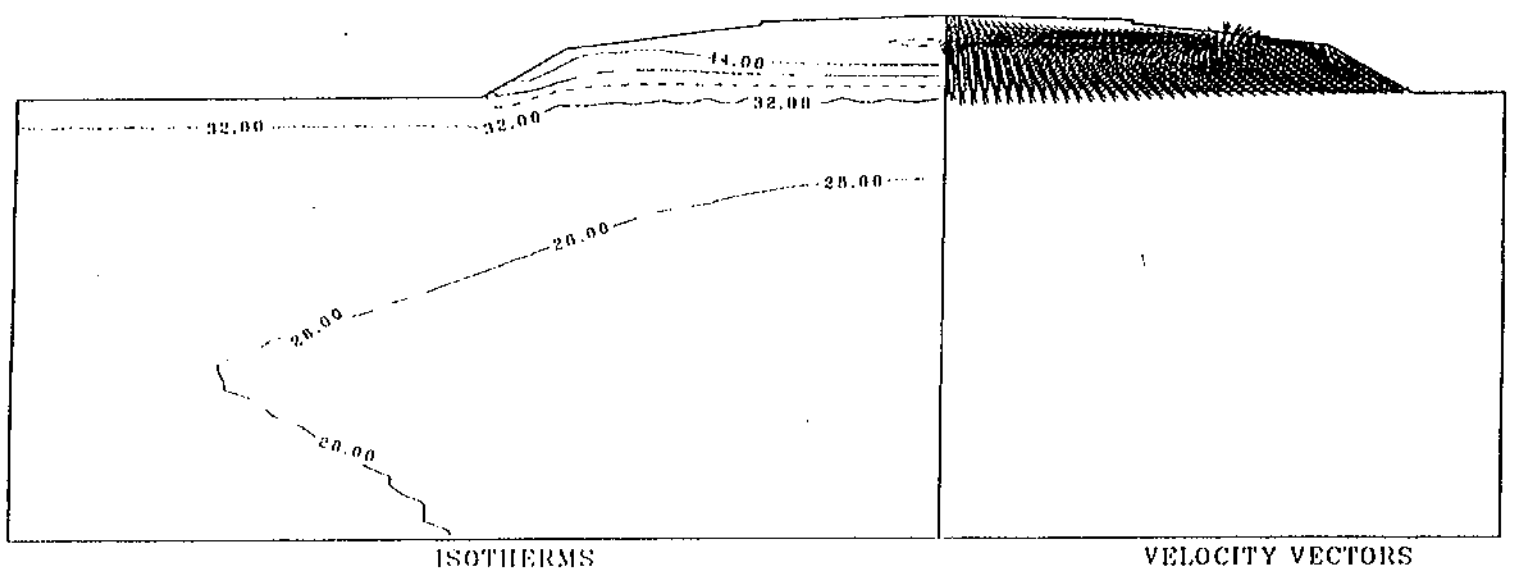


Figure 5(c). Isotherms (°F) and velocity vectors for the Base Case Simulation on September 28.

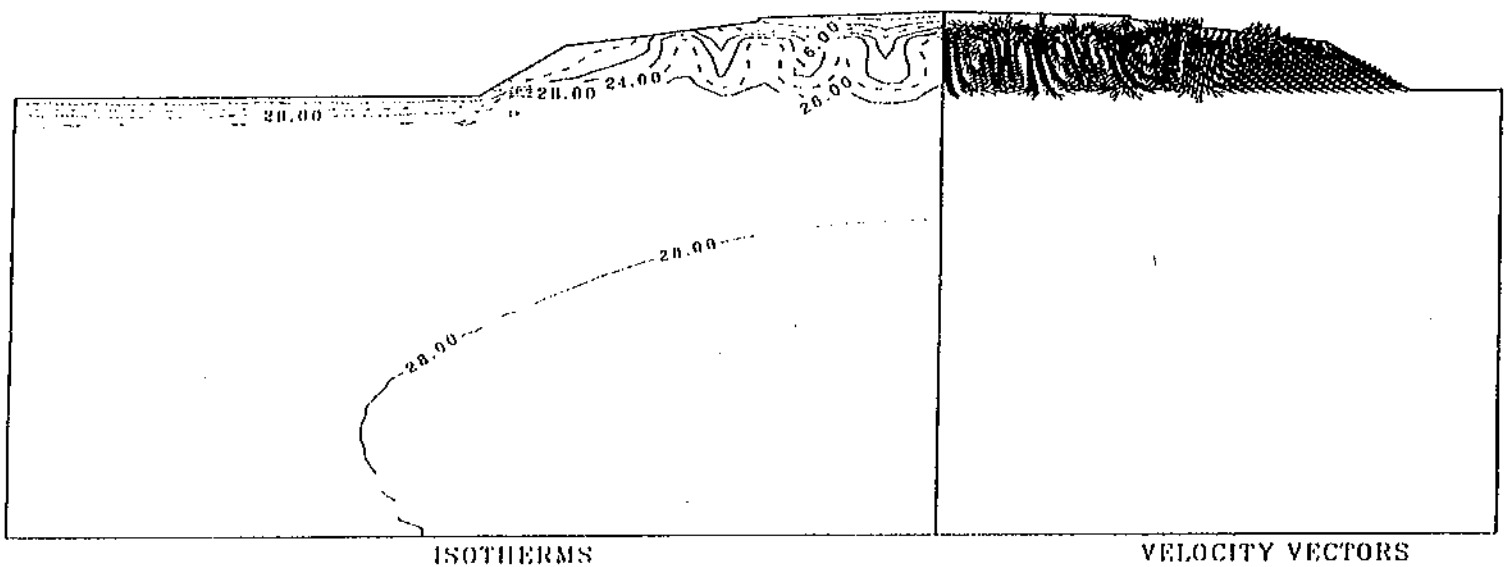


Figure 5(d). Isotherms (°F) and velocity vectors for the Base Case Simulation on November 27.

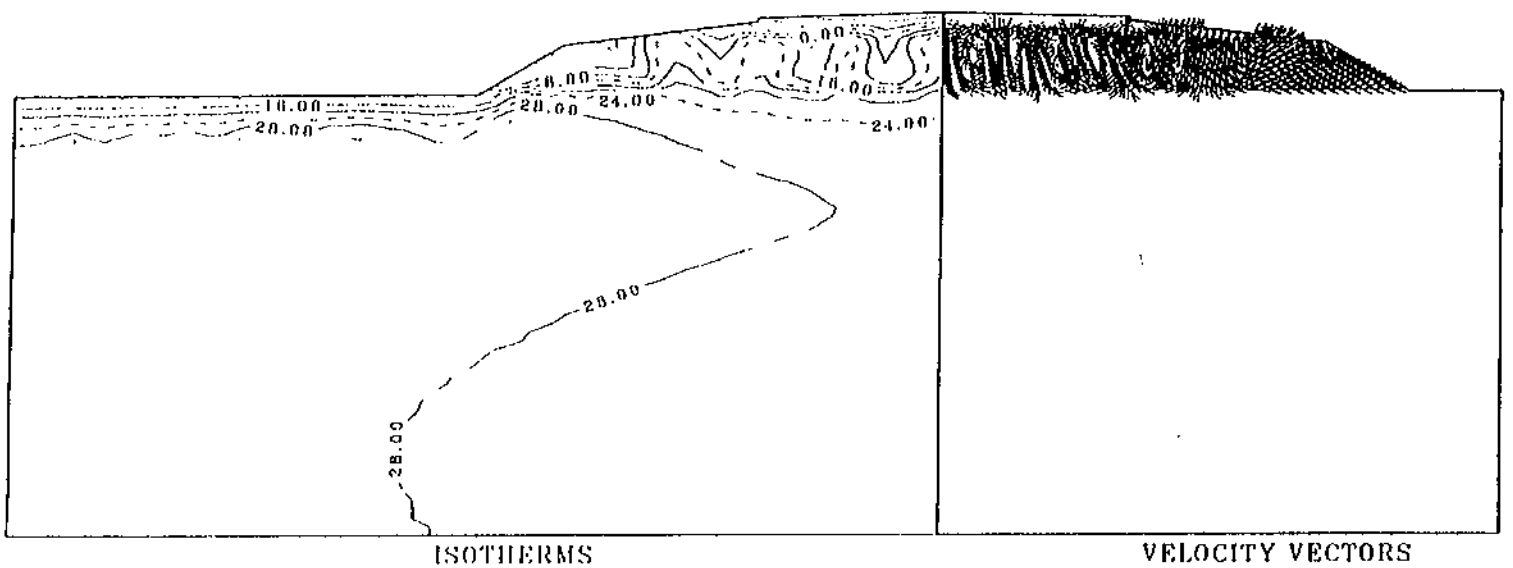


Figure 5(e). Isotherms (°F) and velocity vectors for the Base Case Simulation on January 1.

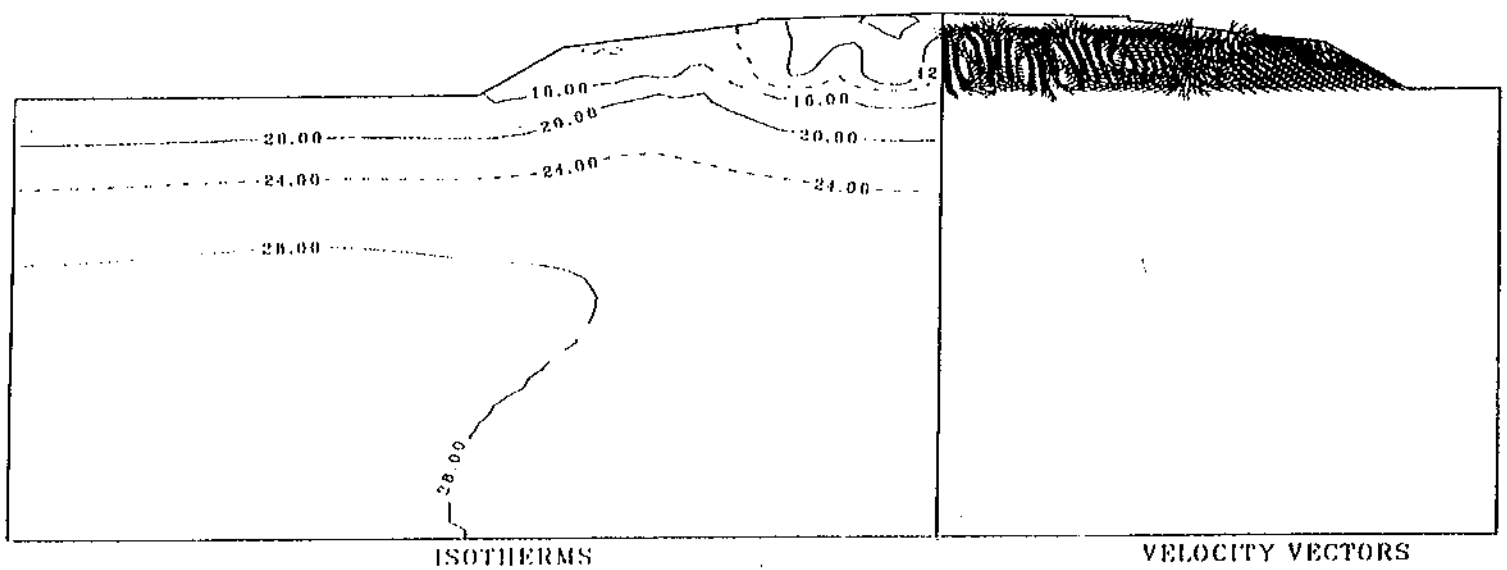


Figure 5(f). Isotherms (°F) and velocity vectors for the Base Case Simulation on March 2.

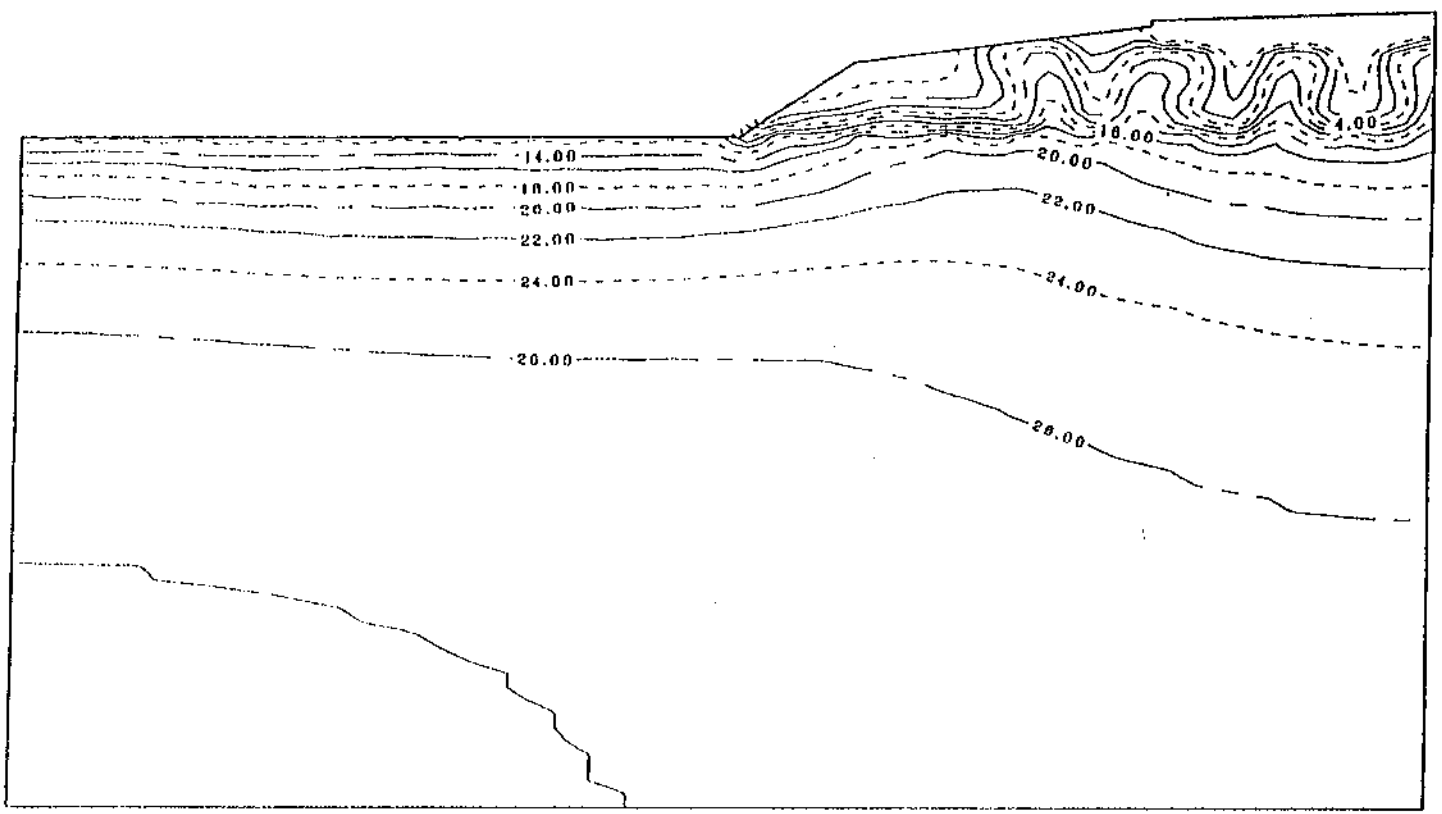


Figure 6. Yearly minimum temperatures (°F) for the Base Case Simulation.

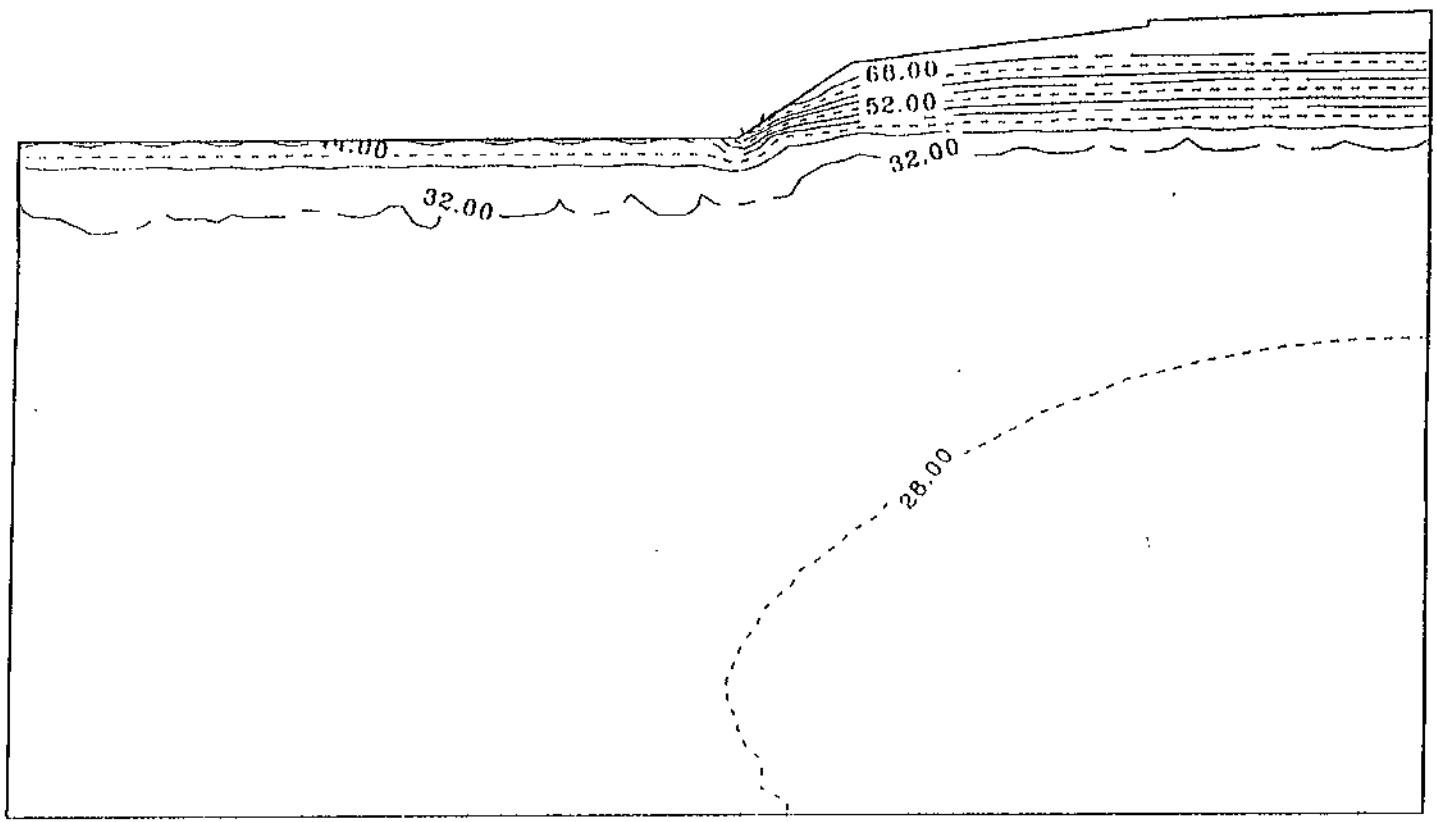


Figure 7. Yearly maximum temperatures (°F) for the Base Case Simulation.

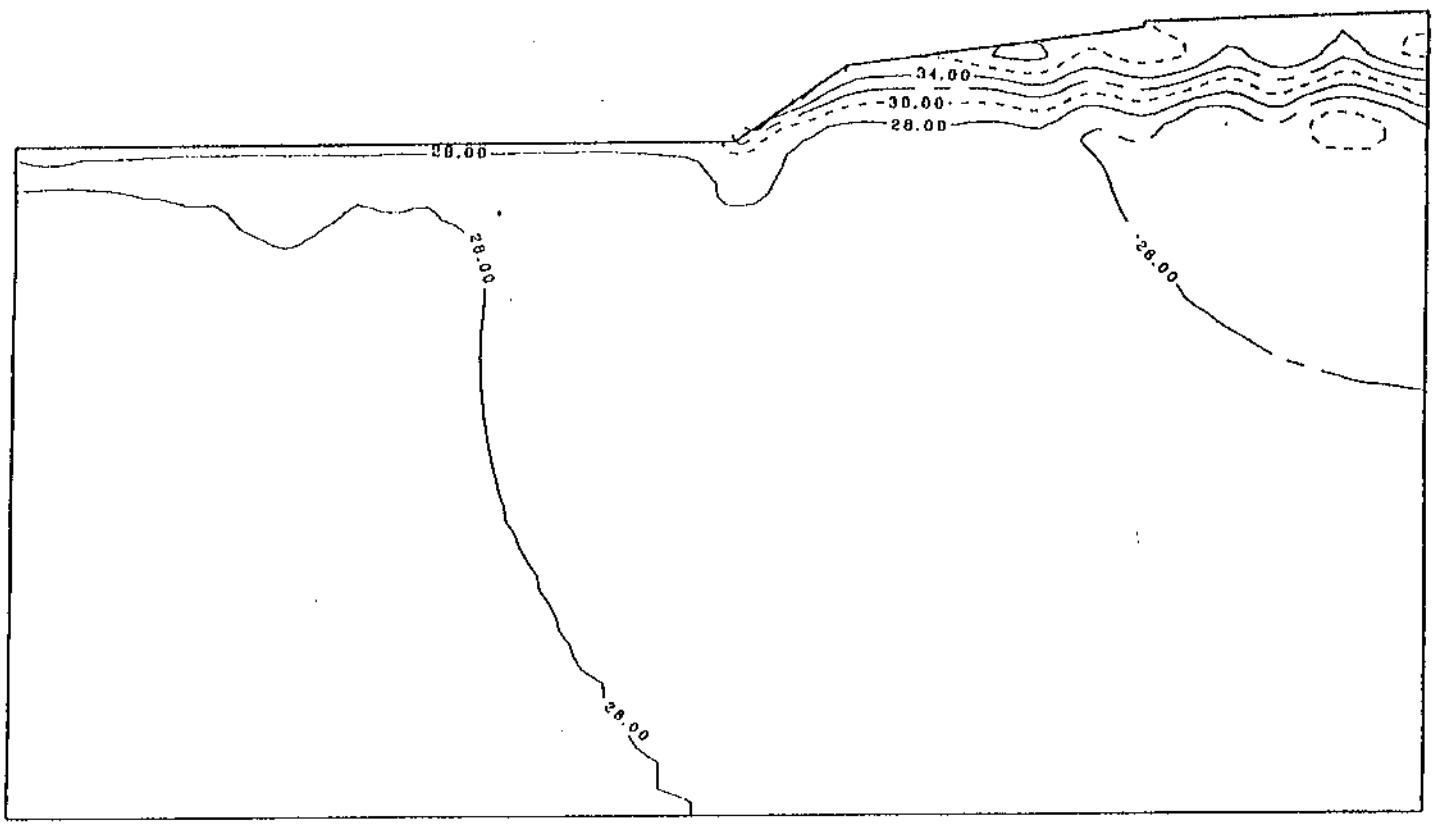


Figure 8. Mean annual temperatures (°F) for the Base Case Simulation.

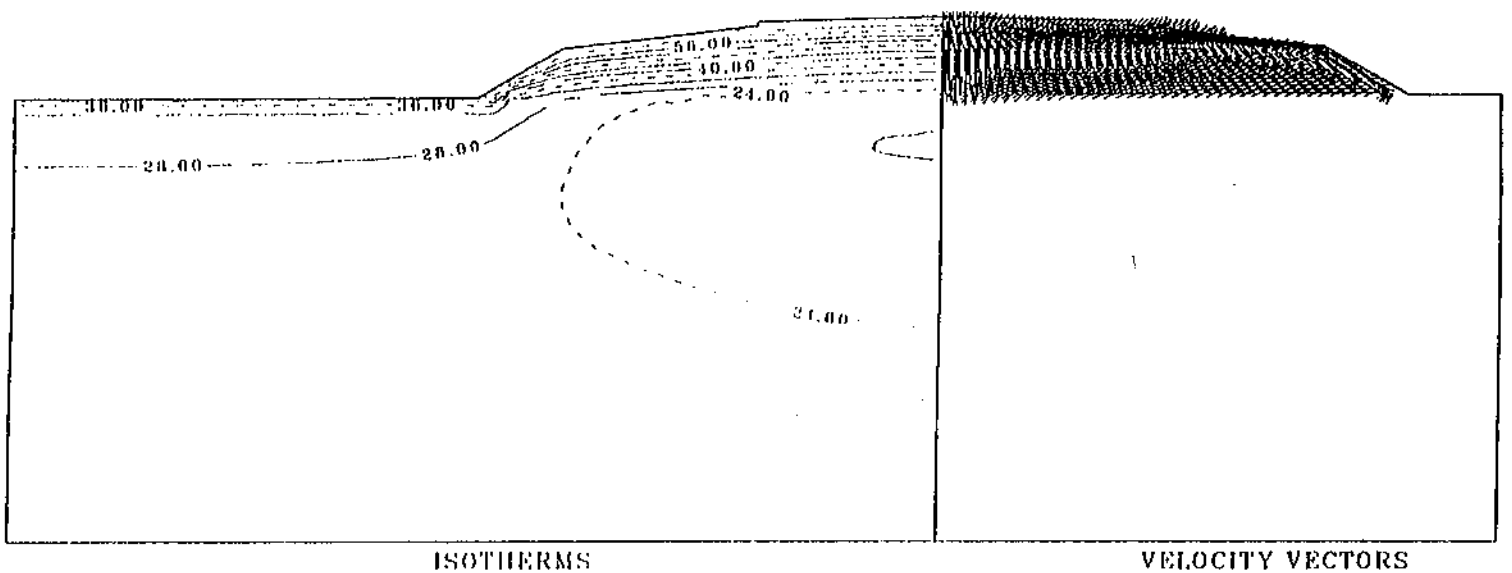


Figure 9(a). Isotherms (°F) and velocity vectors for the 3-Layer Simulation on June 2.

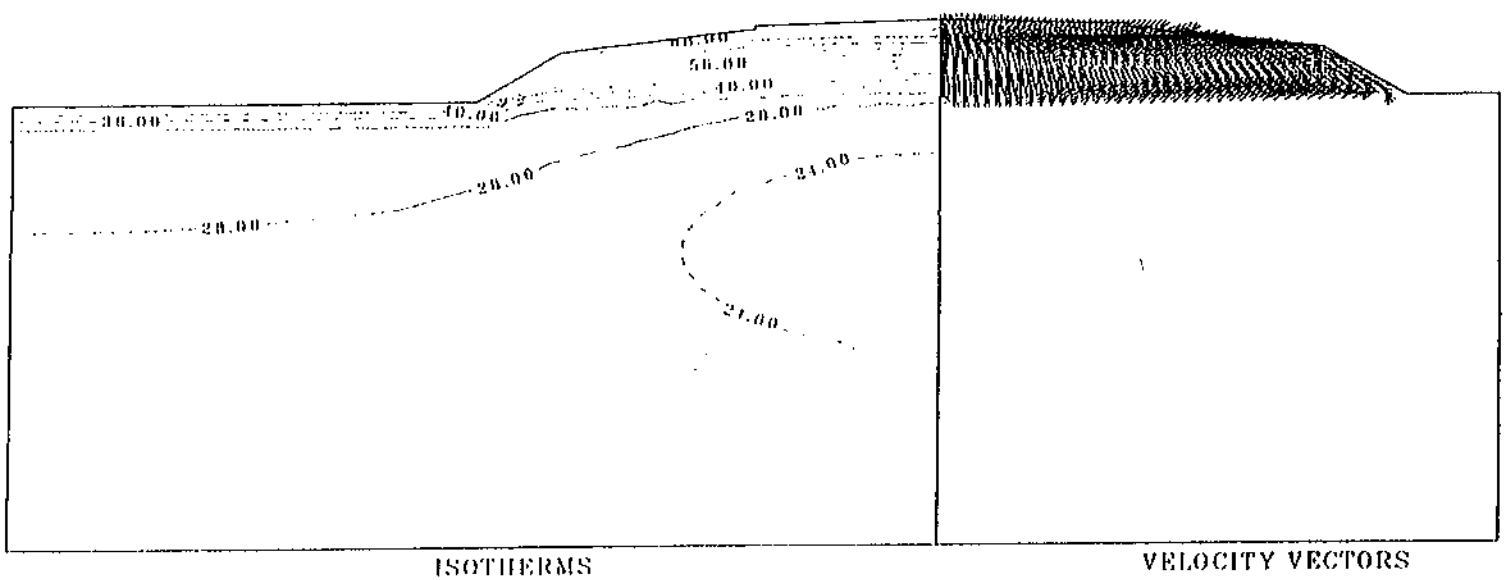


Figure 9(b). Isotherms (°F) and velocity vectors for the 3-Layer Simulation on August 2.

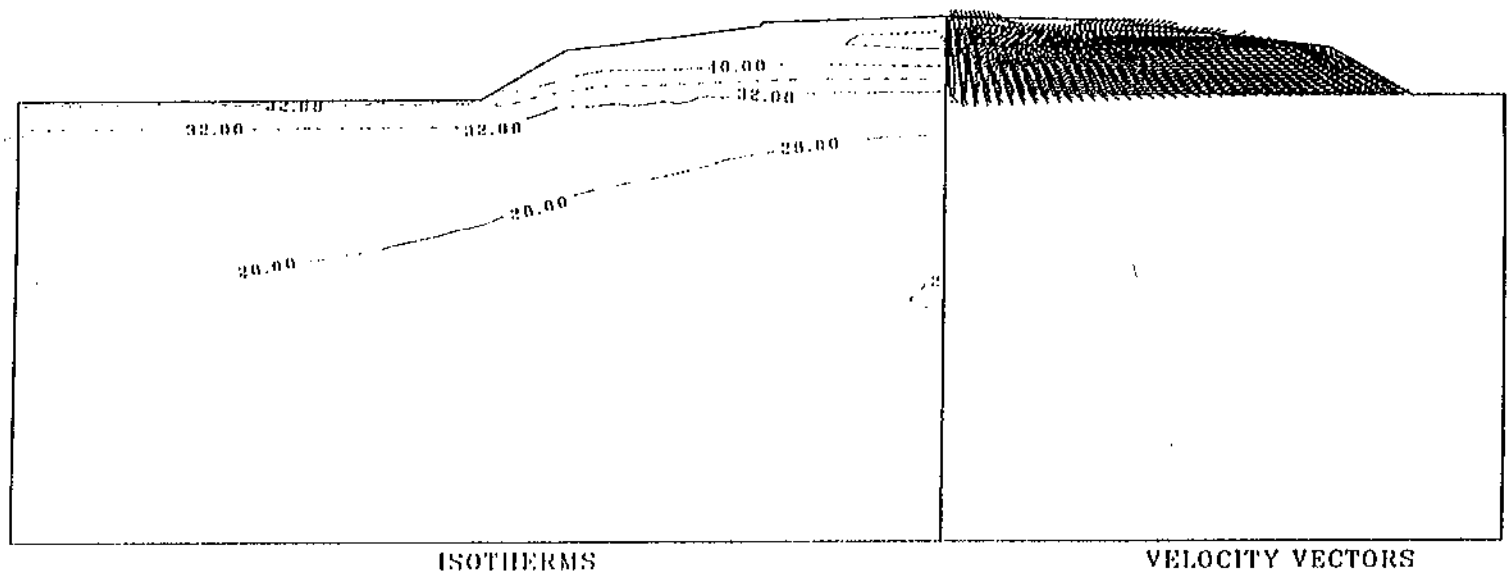


Figure 9(c). Isotherms (°F) and velocity vectors for the 3-Layer Simulation on October 2.

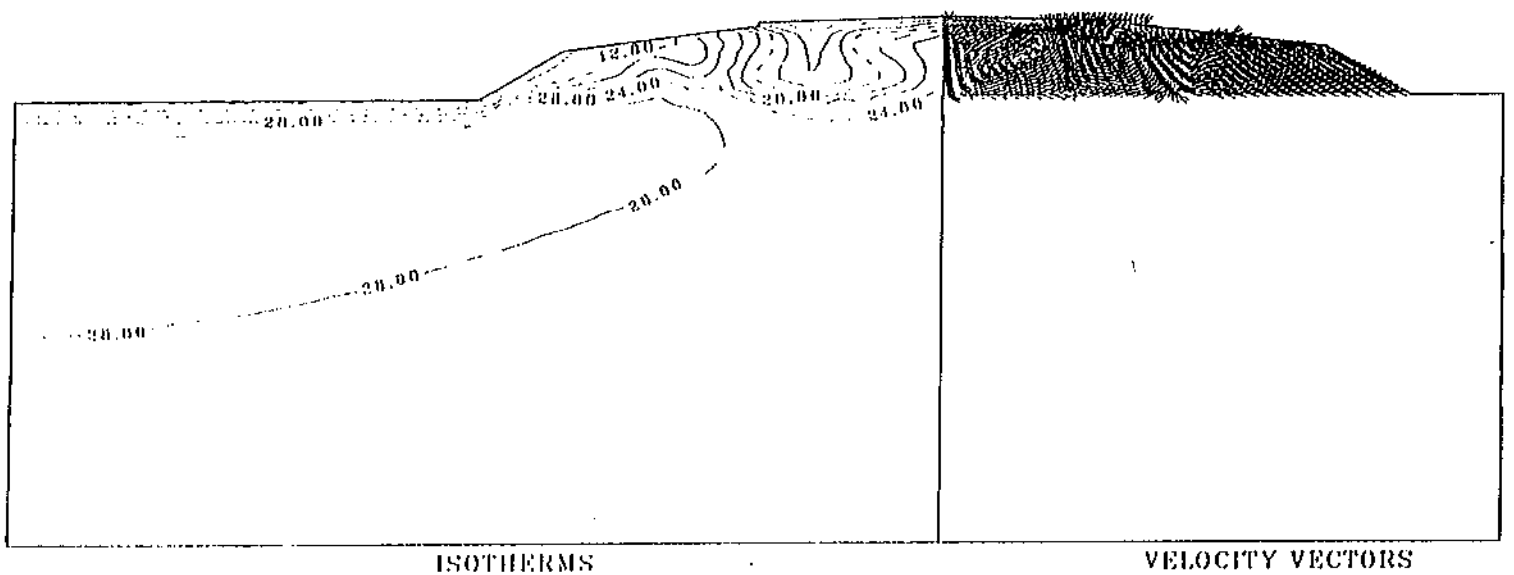


Figure 9(d). Isotherms (°F) and velocity vectors for the 3-Layer Simulation on December 2.

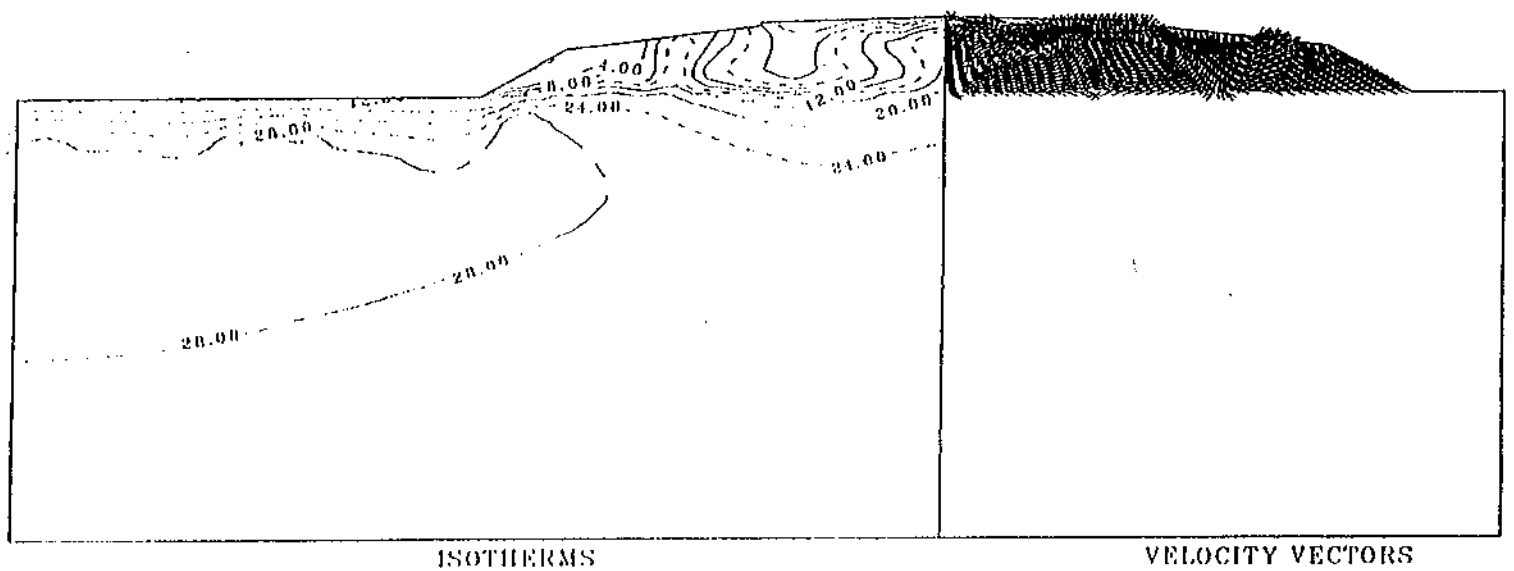


Figure 9(e). Isotherms (°F) and velocity vectors for the 3-Layer Simulation on January 1.

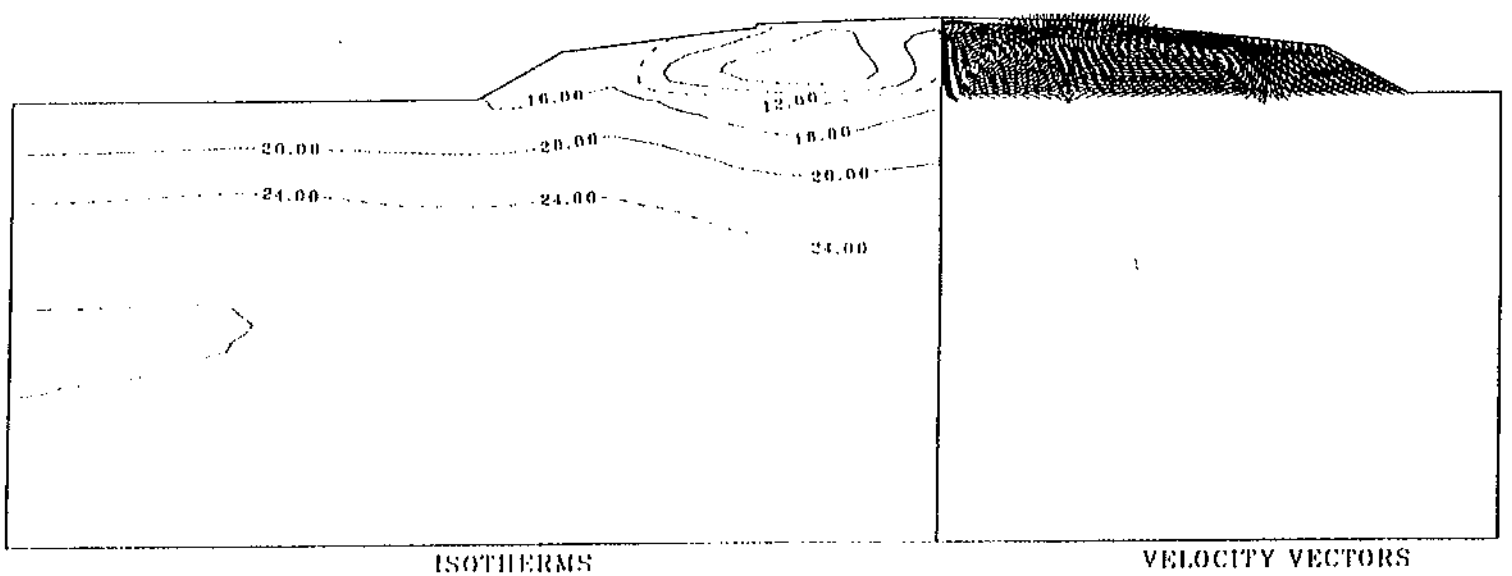


Figure 9(f). Isotherms (°F) and velocity vectors for the 3-Layer Simulation on March 3.

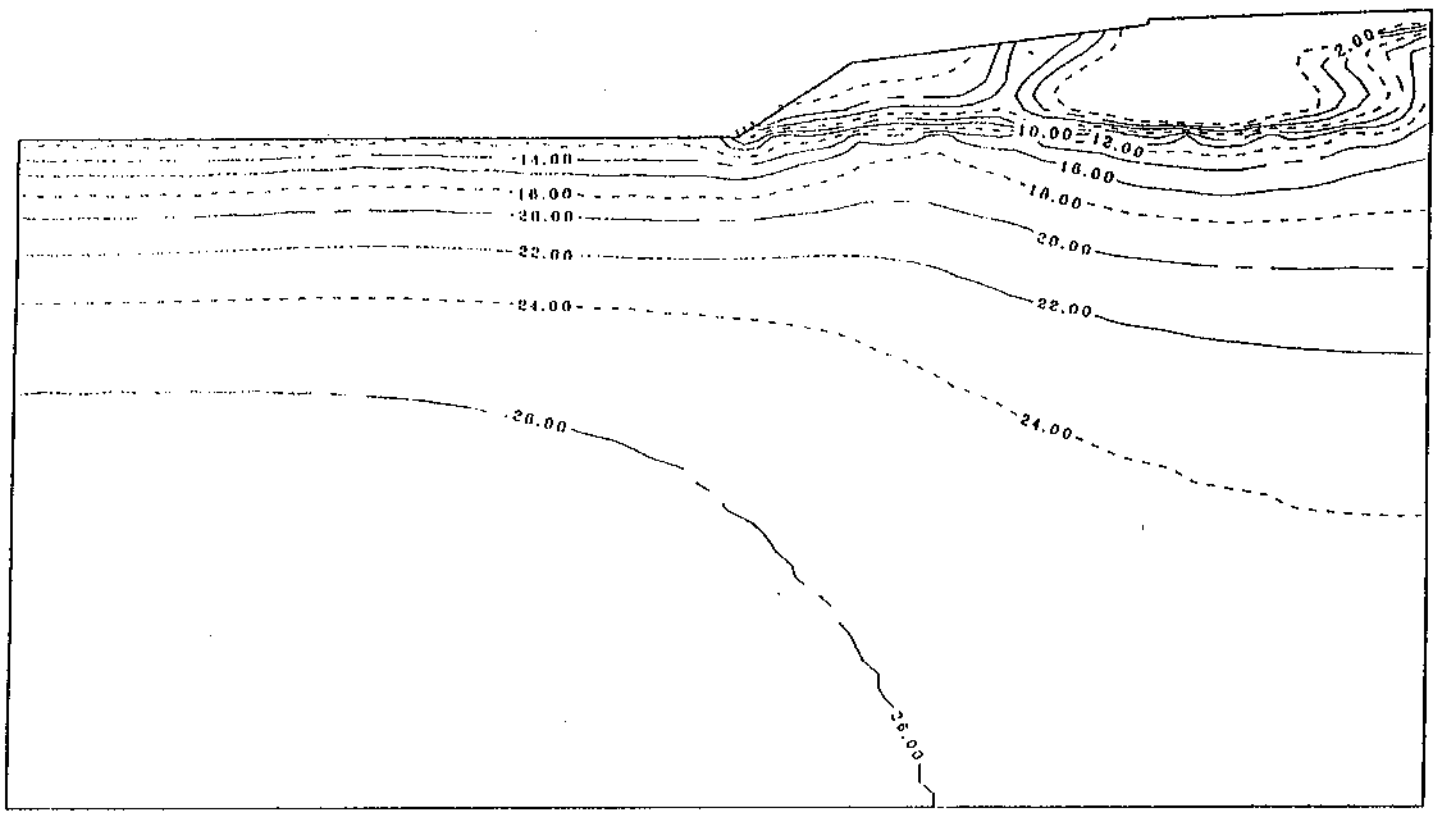


Figure 10. Yearly minimum temperatures (°F) for the 3-Layer Simulation.

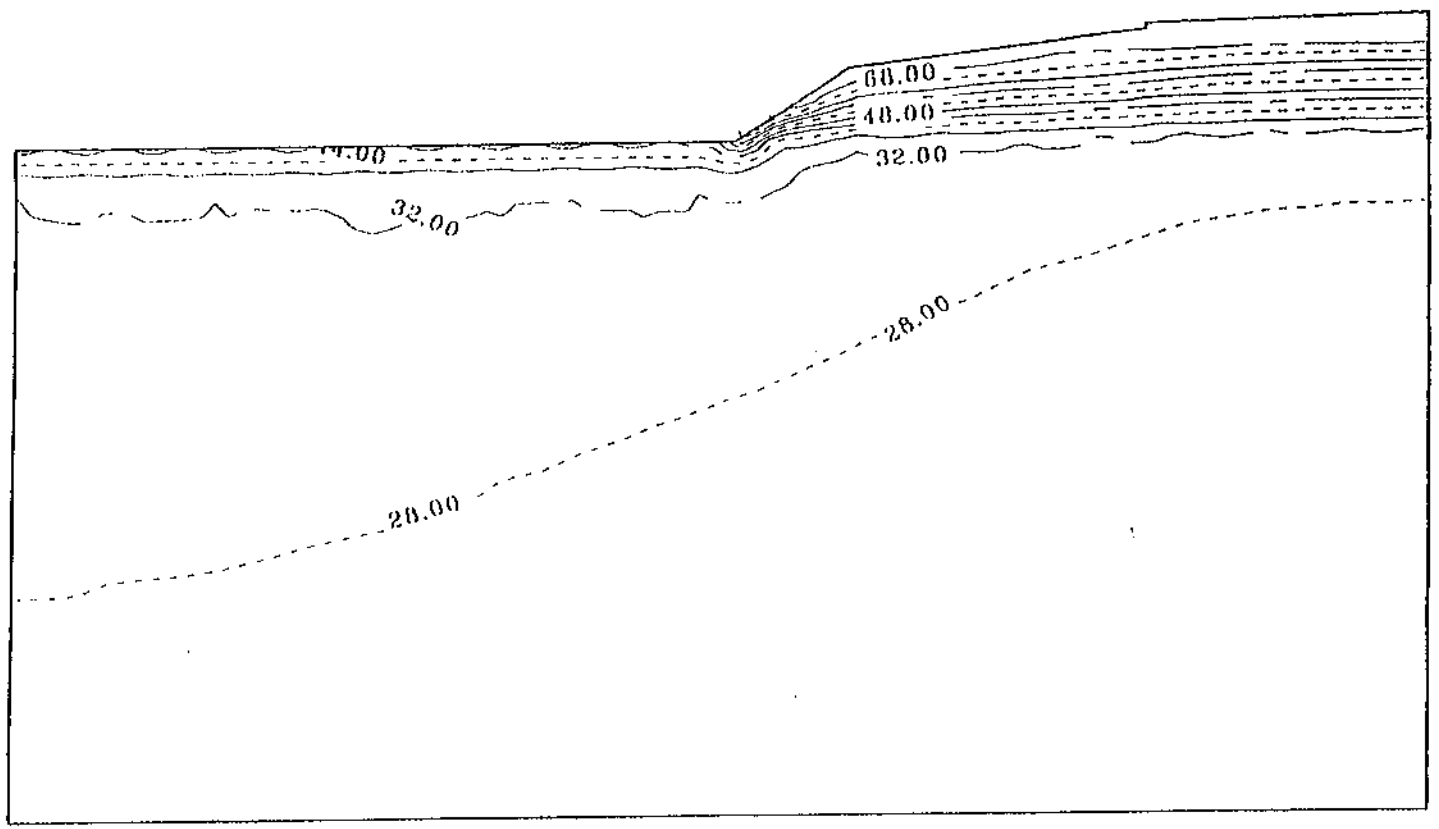


Figure 11. Yearly maximum temperatures (°F) for the 3-Layer Simulation.

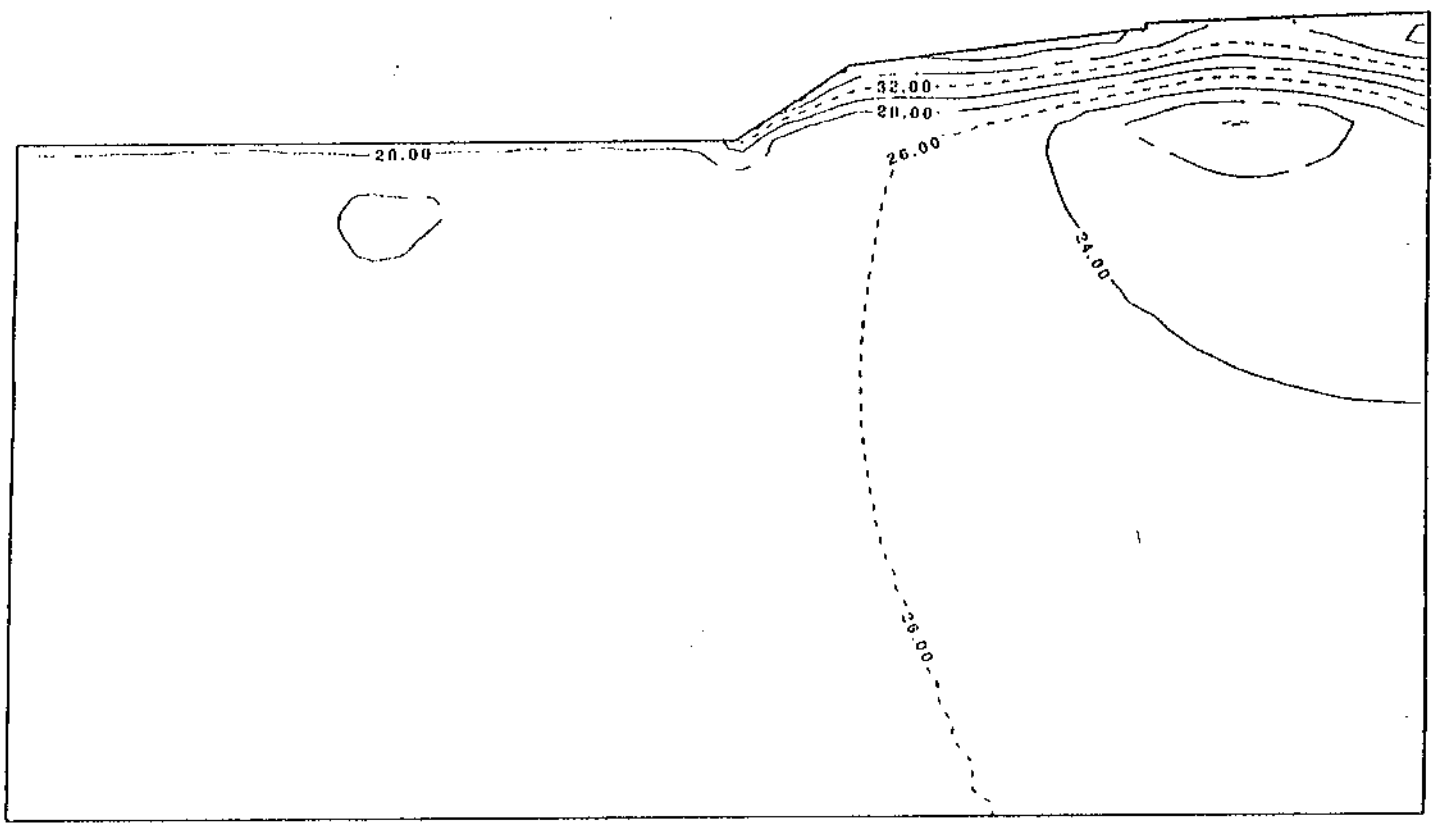


Figure 12. Mean annual temperatures (°F) for the 3-Layer Simulation.

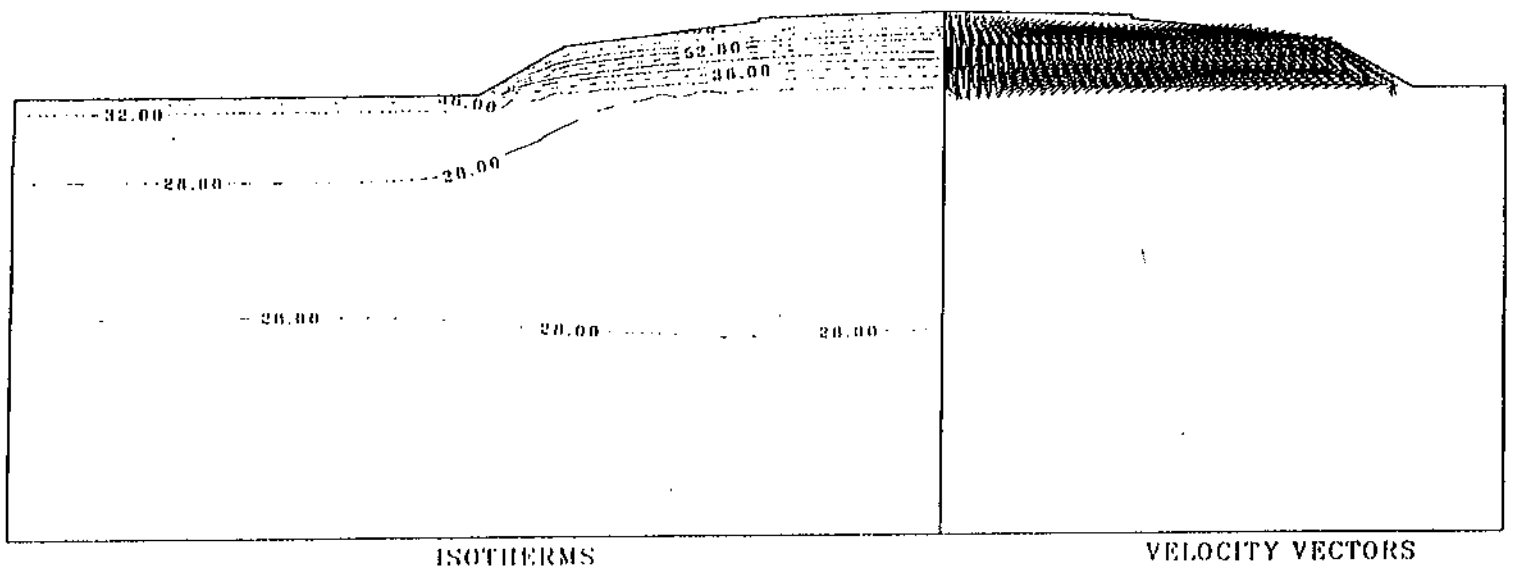


Figure 13(a). Isotherms (°F) and velocity vectors for the Closed Side-Slope Simulation on June 2.

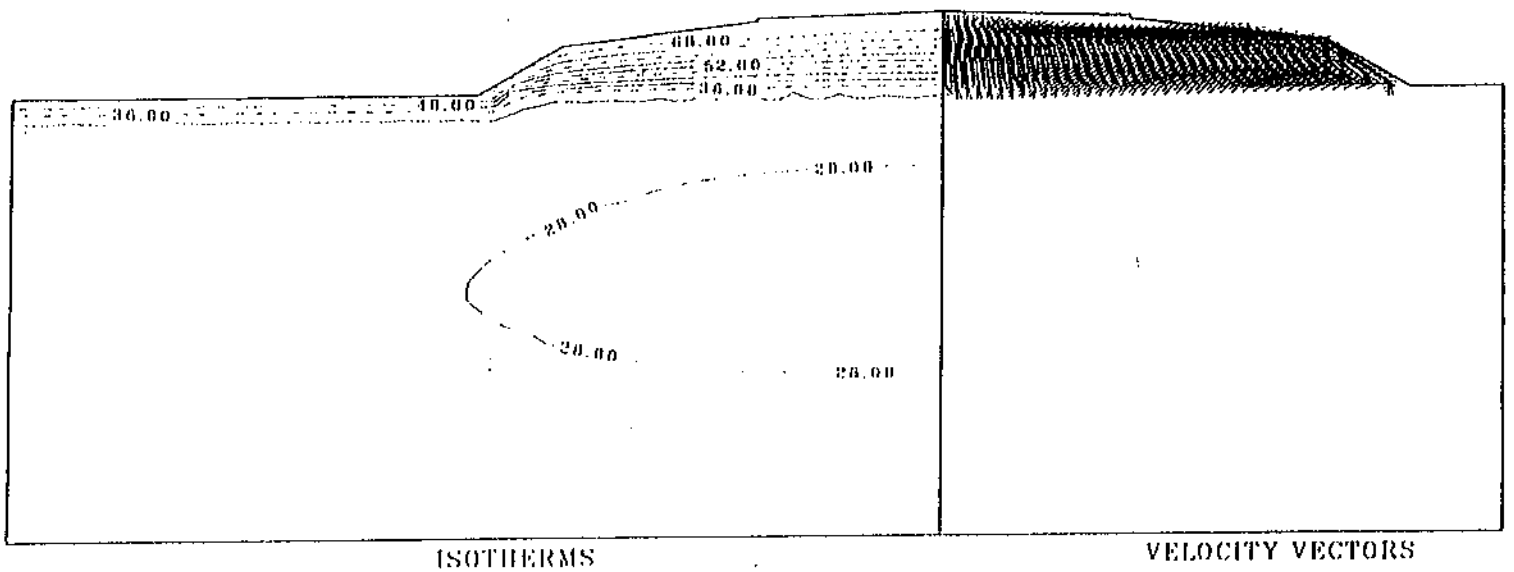


Figure 13(b). Isotherms (°F) and velocity vectors for the Closed Side-Slope Simulation on August 2.

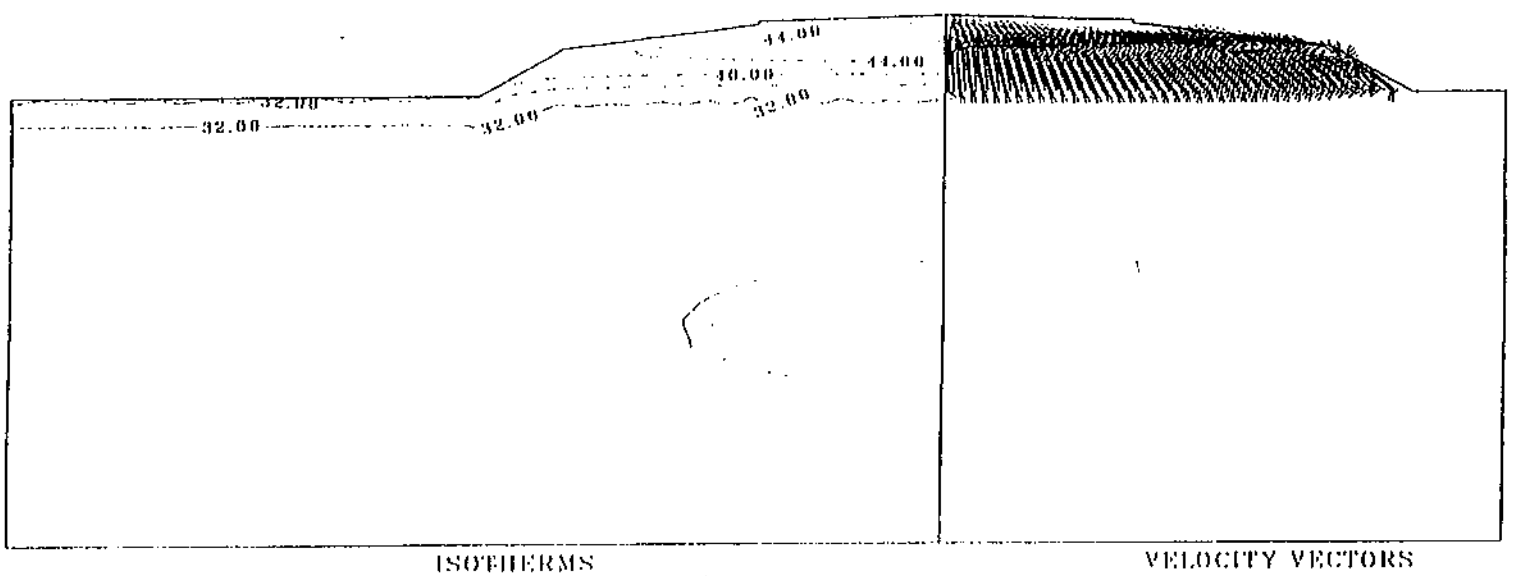


Figure 13(c). Isotherms (°F) and velocity vectors for the Closed Side-Slope Simulation on October 2.

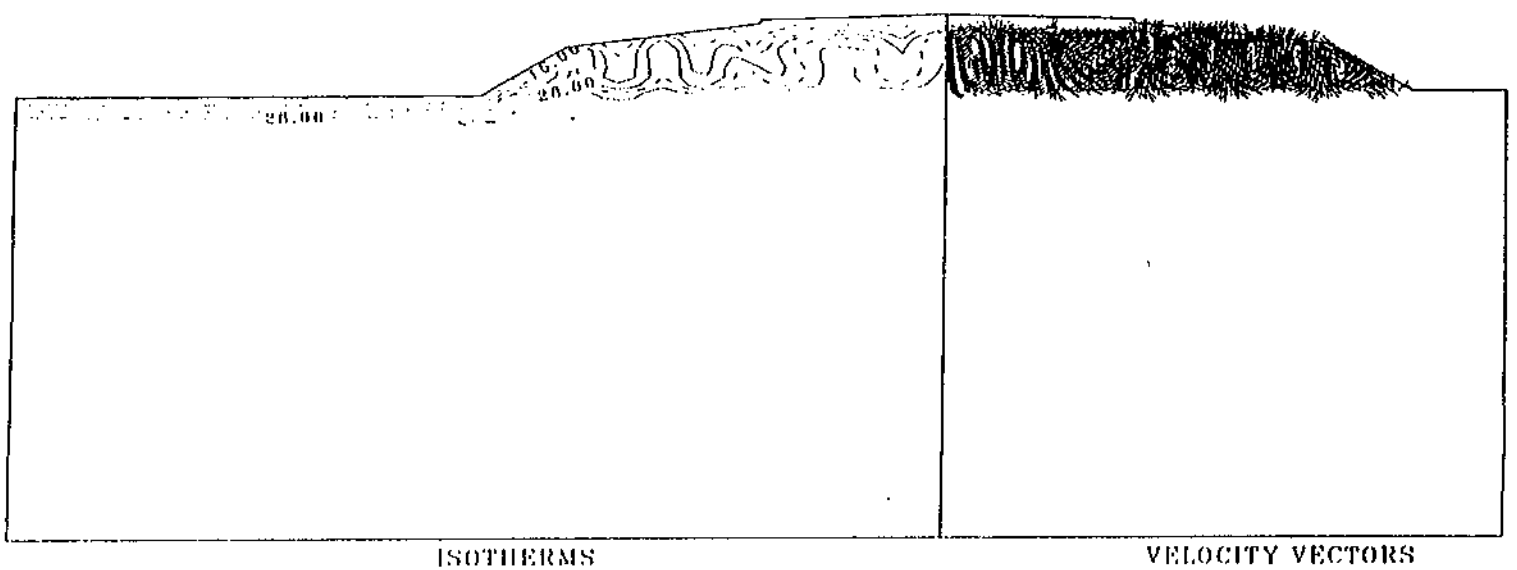


Figure 13(d). Isotherms (°F) and velocity vectors for the Closed Side-Slope Simulation on December 2.

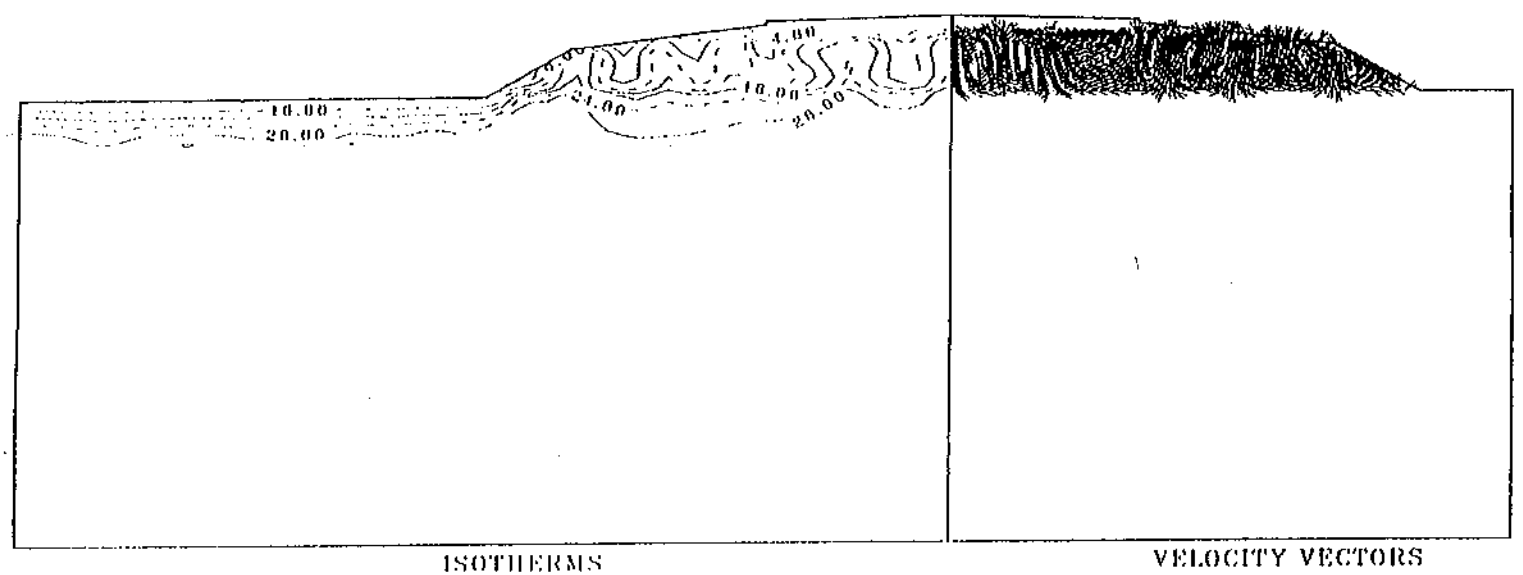


Figure 13(e). Isotherms (°F) and velocity vectors for the Closed Side-Slope Simulation on January 1.

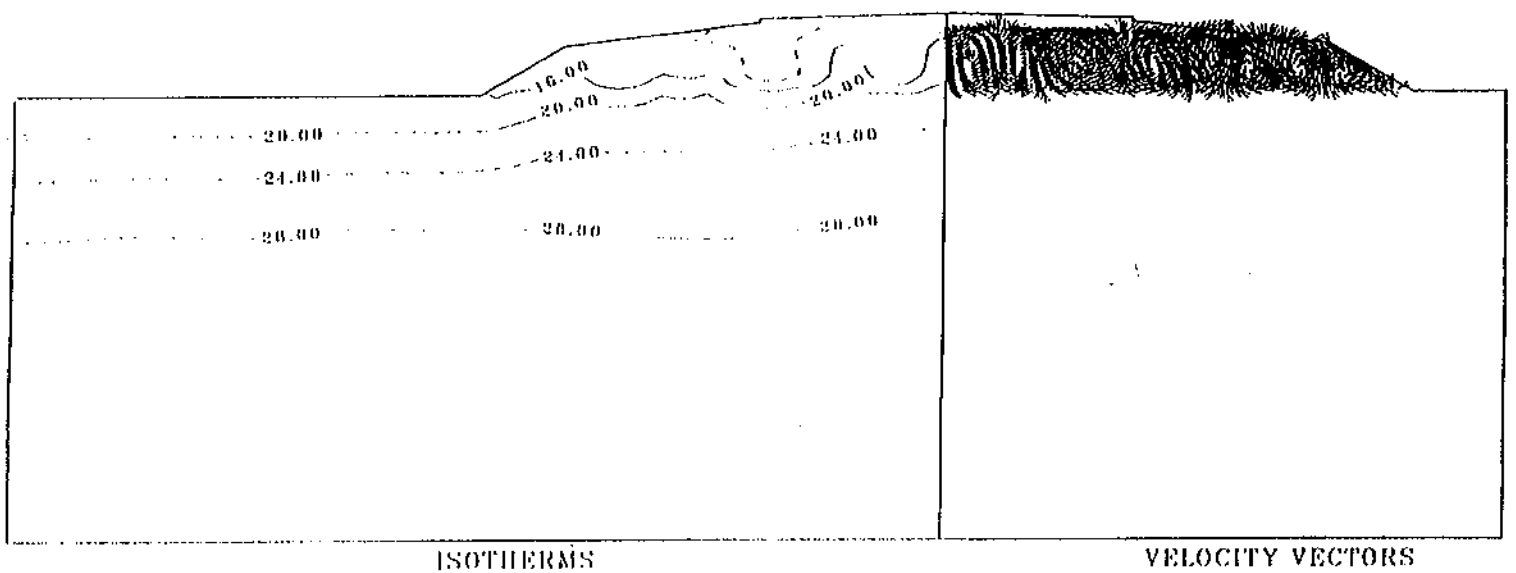


Figure 13(f). Isotherms (°F) and velocity vectors for the Closed Side-Slope Simulation on March 2.

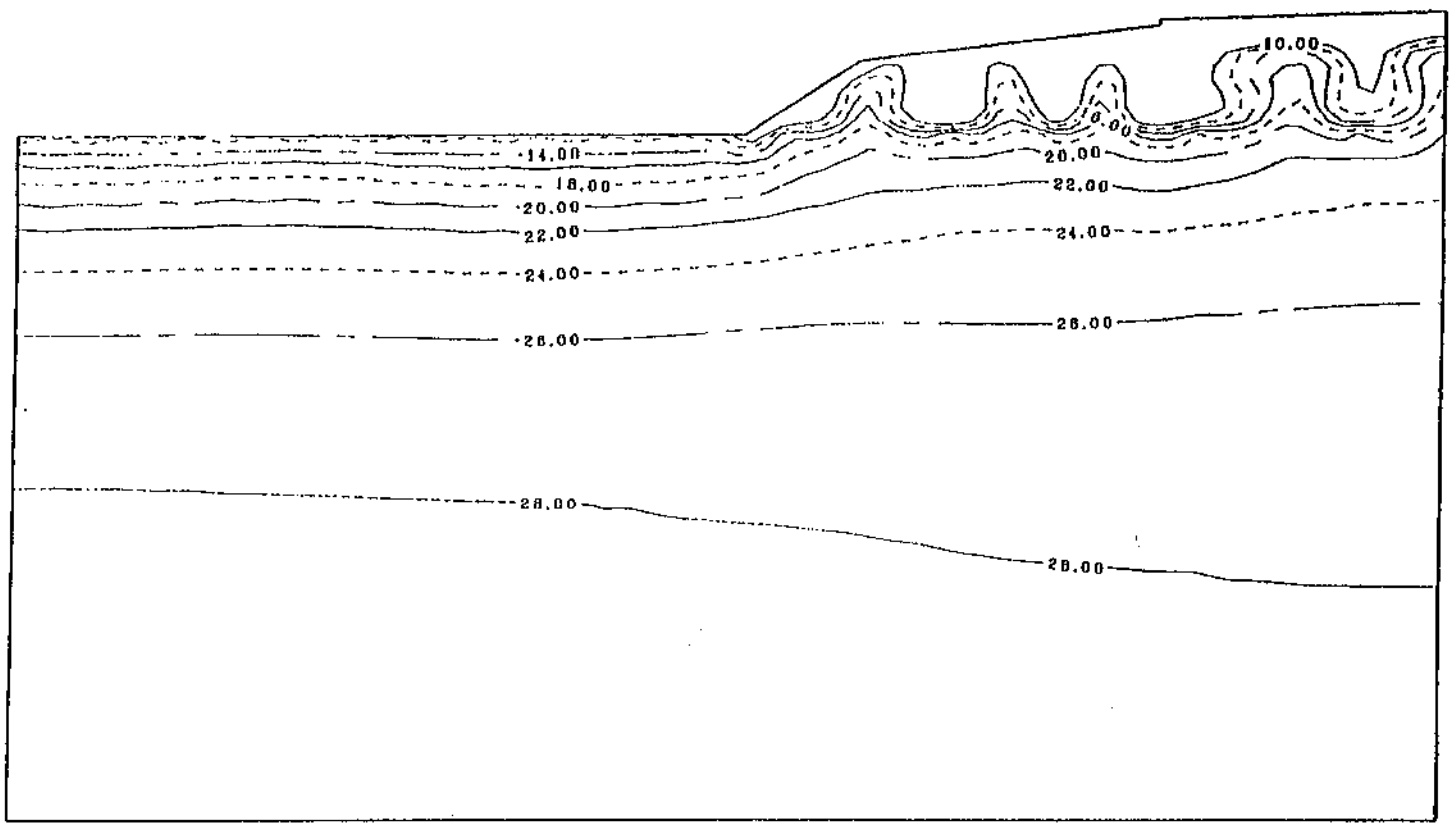


Figure 14. Yearly minimum temperatures (°F) for the Closed Side-Slope Case.

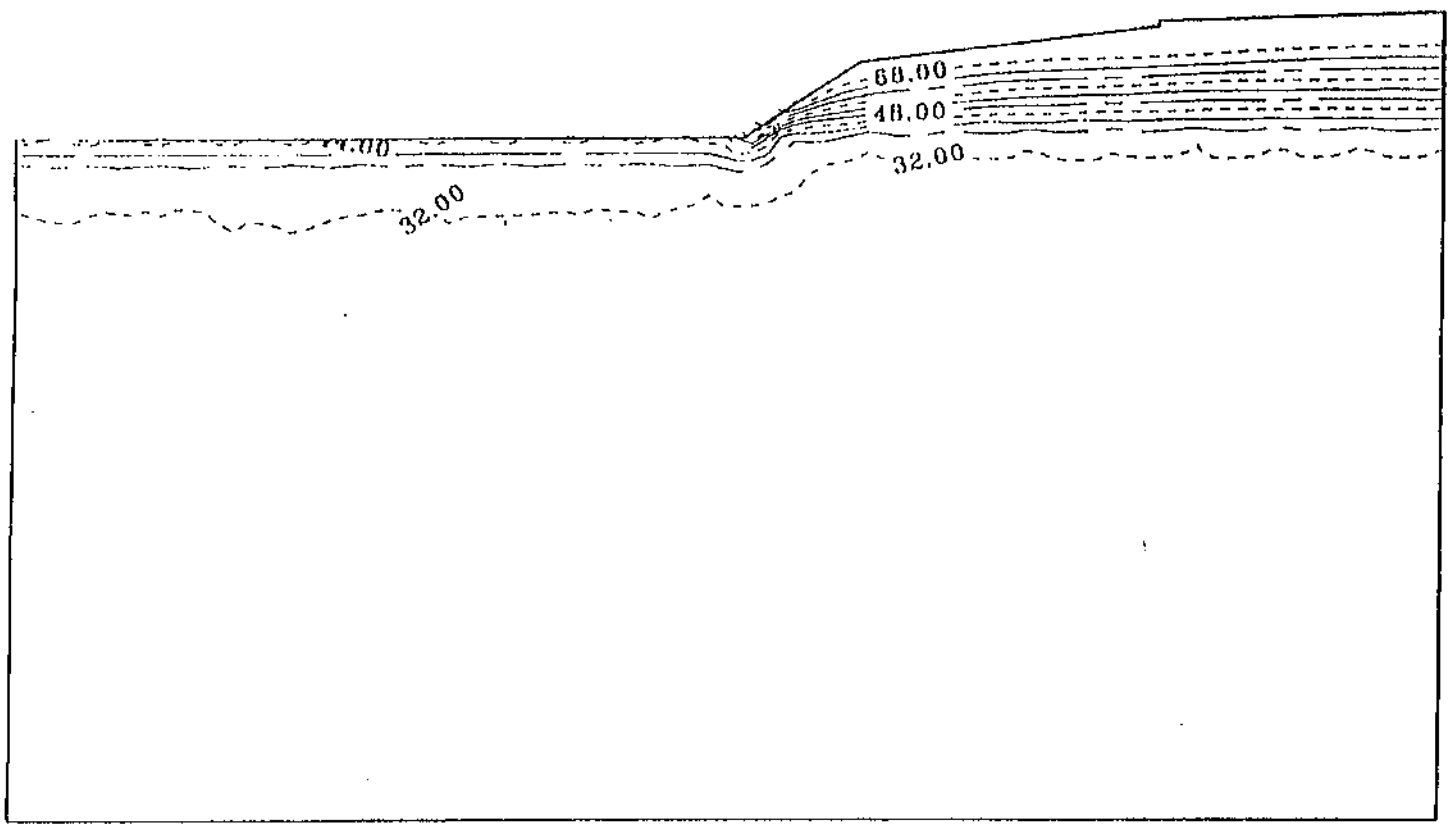


Figure 15. Yearly maximum temperatures (°F) for the Closed Side-Slope Case.

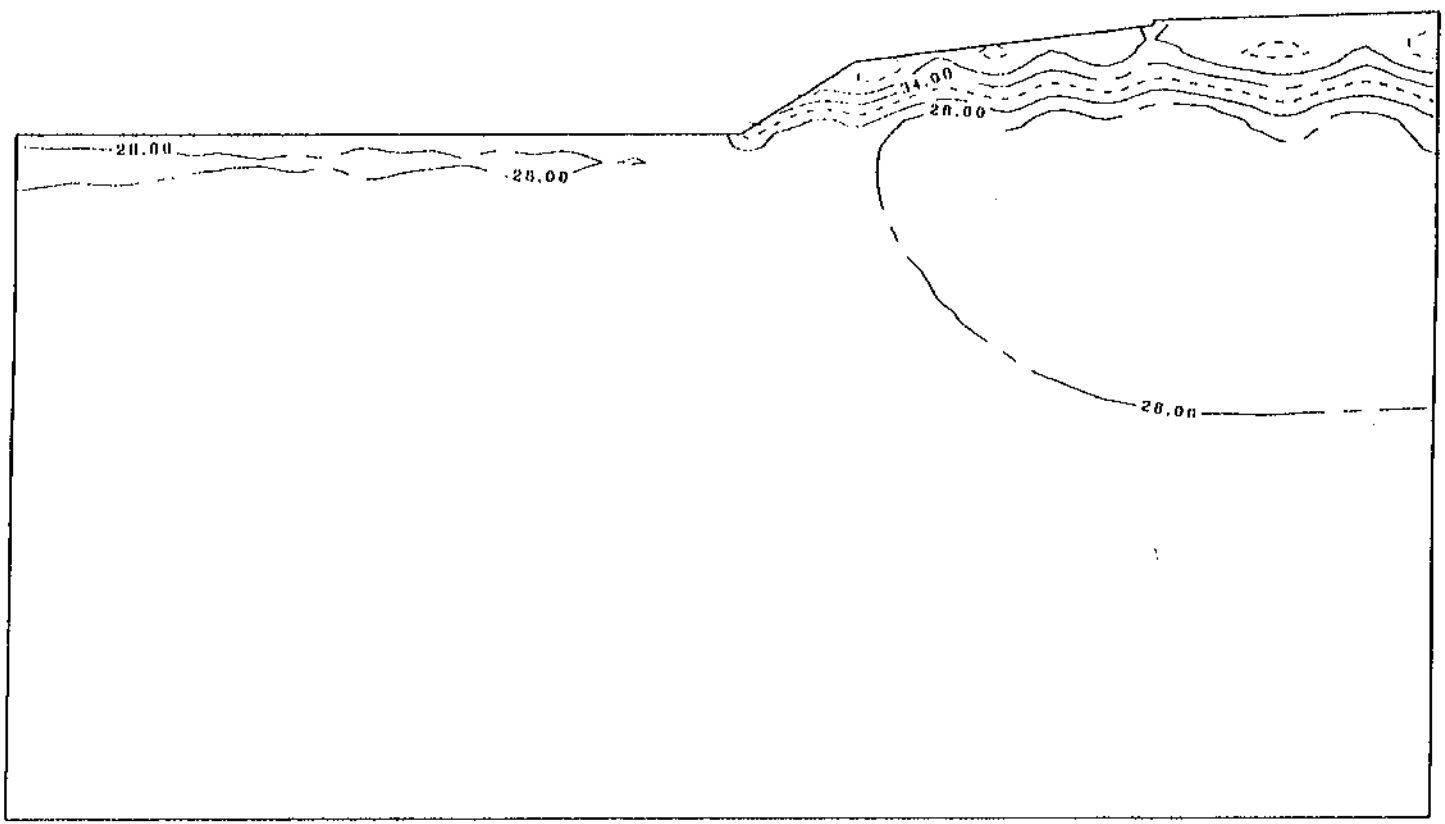


Figure 16. Mean annual temperatures (°F) for the Closed Side-Slope Case.

# 4.0 MATERIAL TESTING/AGGREGATE STUDY

During September of 1996 a series of tests were run at the contractors material site off of Roland Road. These tests were aimed at assessing the air permeability of the large rock which was to be used for the ACE Experimental Feature. The first series of tests were aimed at characterizing the actual gradation curve of the material produced by the contractor's screening process to see if it conformed to the required gradation curve indicated above in Table 1. Three separate gradation tests were run by AKDOT&PF staff. These were accomplished by hand sorting and measuring. The results of the three sample runs are shown in Table 4.

Table 4. Results from Gradation Tests.

| Size | Test 1, % passing | Test 2, % passing | Test 3, % passing | Specification % passing |
|---|---|---|---|---|
| 6 inch (15.2 cm) | 100 | 100 | 100 | 100 |
| 4 inch (10.2 cm) | 100 | 87 | 83 | 5-100 |
| 3 inch (7.6 cm) | 20 | 21 | 29 | 0-5 |
| 1 inch (2.5 cm) | 0.3 | 0.2 | 0.3 | 0-3 |

Table 4 indicates that the material met the 100% passing six inch requirement but that about 20% was passing the three inch screen, which was not within specifications. Despite this, we went ahead and ran permeability tests on the material using a test box with dimensions of 2×2×16 feet. A fan was used to blow air through the box and permeability was obtained using the resulting flow velocities and pressure gradients. A summary of the test results is given in Table 5. In the table, intrinsic permeabilities were calculated two different ways, once using Darcy's Law and once using the

Forchhiemer Equation. It should be noted that this study makes use of an intrinsic permeability (units of length$^2$), instead of a hydraulic conductivity (units of length/time) as is more common when dealing with aquifers and water drainage problems. Darcy's Law is only strictly valid when the pore Reynolds number (labeled Rep in the table) is less than one. In these tests Rep was greater than one, leading to a reduced intrinsic permeability (K) when calculated with Darcy's Law. The Forchhiemer Equation is valid for Rep greater than one and has been used to supplement the Darcy's Law calculations. Forchhiemer's Equation contains an undetermined constant and results have been obtained for two values (0.2 and 0.15). The last column in the table indicates the intrinsic permeability values that were obtained from Forchhiemer's Equation and indicate a conservative K value of approximately $2\times10^{-5}$ ft$^2$ ($1.85\times10^{-6}$ m$^2$). This value is very good, being significantly larger than the permeability we used in our numerical simulations. As a consequence of these tests, our recommendation was to allow the contractor to use the material even though it violated the 5% passing three inch specification. Unfortunately, problems associated with hauling and placement of the material subsequent to our testing generated a large amount of fine material and, consequently, it is felt that these tests do not accurately reflect the permeability of the ACE Experimental Feature as it was actually constructed. Some of the difficulties associated with the actual construction process are discussed in the next section.

Table 5. Results from Field Air Permeability Tests.

ACE Material Permeability Tests at Roland Rd. Pit, 9/13/96, Air temp = 45F

| | |
|---|---|
| Air density ($lb_m/ft^3$) | 0.0794 |
| Viscosity ($lb_m/s\ ft$) | 1.174E-05 |
| Forch. const. | 0.2 |

| Description | Del. P in $H_2O$ | Velocity ft/s | dP/dx $lb/ft^2/ft$ | K Darcy $ft^2$ | Rep Darcy | K Forch. $ft^2$ |
|---|---|---|---|---|---|---|
| 8" orifice, Variac 140 | 0.148 | 0.754 | 0.0551 | 4.989E-06 | 11.40 | 3.522E-05 |
| 8" orifice, Variac 70 | 0.0275 | 0.322 | 0.0102 | 1.152E-05 | 7.41 | 4.545E-05 |
| 4" orifice, Variac 70 | 0.0153 | 0.186 | 0.00569 | 1.193E-05 | 4.35 | 2.779E-05 |
| 4" orifice, Variac 50 | 0.00944 | 0.127 | 0.00350 | 1.331E-05 | 3.15 | 2.476E-05 |

| | |
|---|---|
| Air density ($lb_m/ft^3$) | 0.0794 |
| Viscosity ($lb_m/s\ ft$) | 1.174E-05 |
| Forch. const. | 0.15 |

| Description | Del. P in $H_2O$ | Velocity ft/s | dP/dx $lb/ft^2/ft$ | K Darcy $ft^2$ | Rep Darcy | K Forch. $ft^2$ |
|---|---|---|---|---|---|---|
| 8" orifice, Variac 140 | 0.148 | 0.754 | 0.0551 | 4.989E-06 | 11.40 | 2.351E-05 |
| 8" orifice, Variac 70 | 0.0275 | 0.322 | 0.01021 | 1.152E-05 | 7.41 | 3.331E-05 |
| 4" orifice, Variac 70 | 0.0153 | 0.186 | 0.00569 | 1.193E-05 | 4.35 | 2.268E-05 |
| 4" orifice, Variac 50 | 0.00944 | 0.127 | 0.00350 | 1.331E-05 | 3.15 | 2.127E-05 |

# CHAPTER 5. EMBANKMENT CONSTRUCTION

Construction of the section of the Parks/Chena Ridge Interchange Project which includes the ACE experimental feature began in mid September of 1996. Due to the permafrost nature of the soils in this portion of the project area, construction activities were required to commence after September 15 to avoid unnecessary thawing of the foundation soil. Clearing of the area was carried out using a "Hydro Ax" and much of the brush was left lying on the surface. Clearing was accomplished with minimal disturbance to the existing moss mat with the hope that this would also help to limit thermal disturbance of the underlying soils. Once clearing and surveying operations were complete the contractor began material placement. The first step in construction of the ACE experimental feature consisted of placing a borrow embankment up to each side of the ACE test section. In order to avoid driving across the ACE section after it was completed, the contractor also built single-lane borrow embankments on each side of the ACE test section to allow construction equipment to pass. Figure 17 shows the test section site after the clearing operation was complete.

Placement of the ACE rock layer began on approximately September 20. Initially placement of the rock was carried out according to the construction specifications, which called for placement in 2 ft. (0.61 m) lifts using a rubber-tired loader. After approximately 50% of the rock layer had been placed it was noticed that the loader was causing material degradation below the surface layer. It is presumed that this was caused by the tires loading the rock at the surface and generating a grinding action

between the surface rock and the rock lower down. This degradation was not apparent from the surface, but was only noticed when the subsurface layers were probed. The main difficulty was that the action of the loader had caused a uniform layer of fine material to be generated. Figure 18 shows the layer of fines which was found below the surface. It was feared that this layer of fine material would interrupt the convection in the embankment and reduce the cooling effectiveness. In order to improve the situation, the contractor offered to "sift" the rock using a large back hoe. The hoe operator was able to reach from each end of the test section out into the middle of the test section, pick up a bucket of the rock material, shake it to sift the fines to the bottom of the bucket, and then pour the rock back out with the fines remaining at the bottom of the bucket. The fines were then deposited at each end of the test section. This operation appeared to be successful in removing and breaking up the layer of fines which had developed.

Initially, the contractor placed ACE rock material from each end of the test section up to the middle and then left a V-notch at the center cross-section to allow the instrumentation to be installed. This instrumentation included three vertical and five horizontal thermistor strings (as shown in Figure 1). The vertical strings labeled D, E, and F were installed using a drill rig and the cables were then routed to the side of the embankment in schedule 80 PVC electrical conduit. Figure 19 shows the drilling operation in progress. Once the vertical strings were installed beneath the base of the embankment, the horizontal strings (labeled G, H, I, J, and K) were installed one at a time while ACE rock was placed over each one in turn. The cables for these strings were again routed to the side of the embankment and eventually into a junction box.

Figure 20 shows one of the horizontal thermistor strings being installed in the embankment. Once the instrumentation had been installed the surface of the embankment was leveled and left without any covering over the ACE rock for winter. During the spring and summer of 1997 the ACE test section was finished by covering the rock with a the choke layer and then asphalt with a treated base beneath it. The finished test section is shown in Figure 21.

There were a number of lessons learned during the construction of this test section. Probably the most important involved methods for placement of the ACE rock layer. In future installations, it would be preferable to allow the contractor to place the ACE rock material in a single lift by simply dumping the material and then pushing it forward from the existing roadbed. This would eliminate the need to drive on each lift as it is placed. Driving on the surface of the ACE rock should be minimized as much as possible and, if necessary, it is preferable to drive only on the finish elevation instead of driving on the surface of several smaller lifts. If driving on the surface is required during construction, it is probably better to use tracked equipment (CATs) rather than rubber-tired equipment. Tracks would tend to distribute the weight of the equipment more uniformly over the rock. While it is possible that steel tracks will degrade material at the surface, it is less likely that material beneath the surface will be broken because of the improved weight distribution.

Figure 17. Early stages of construction showing cleared area and initial placement of ACE embankment material.

Figure 18. Layer of fines generated during embankment construction.

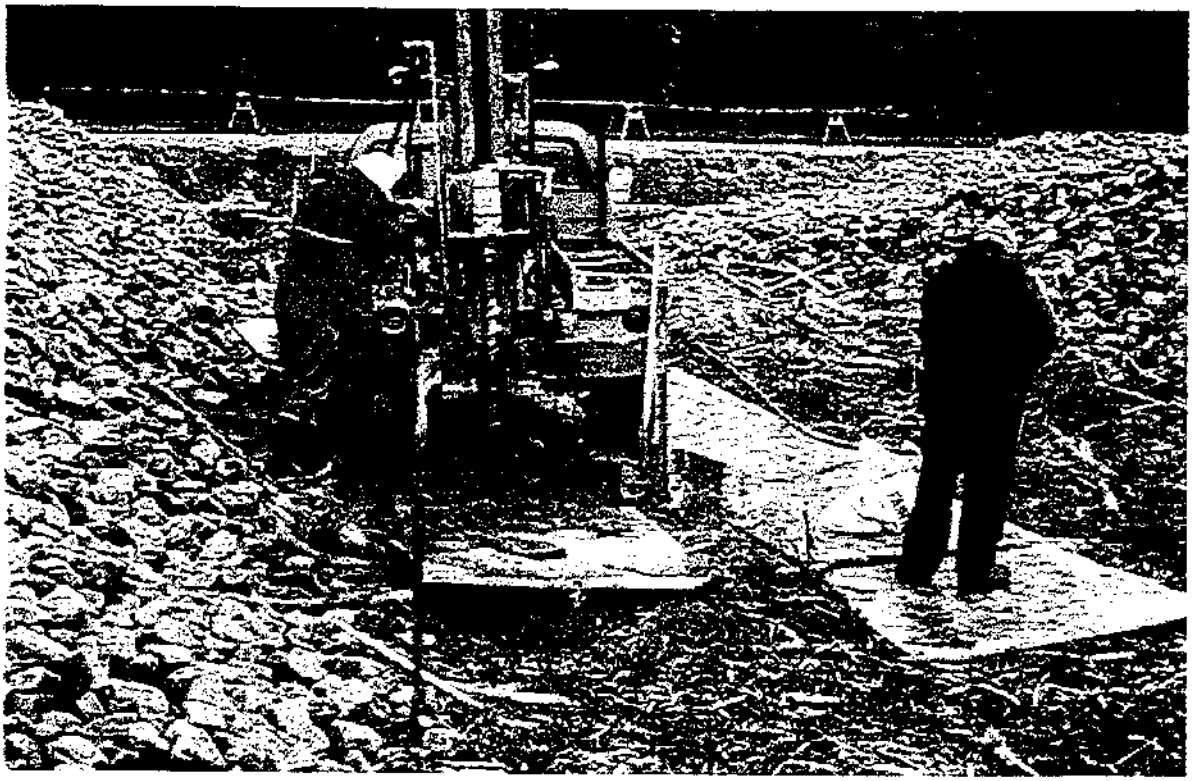

Figure 19. Installation of vertical thermistor strings beneath the test section.

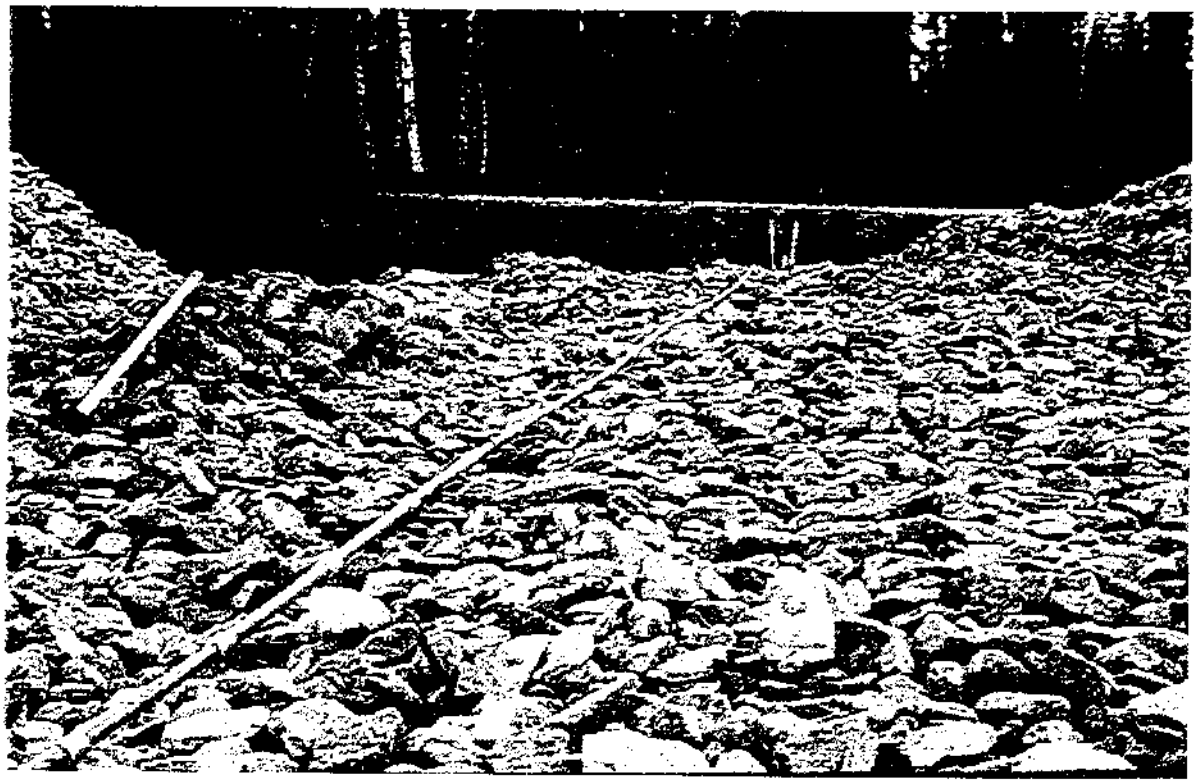

Figure 20. Installation of horizontal thermistor strings within the test section. Aluminum shield rings shown.

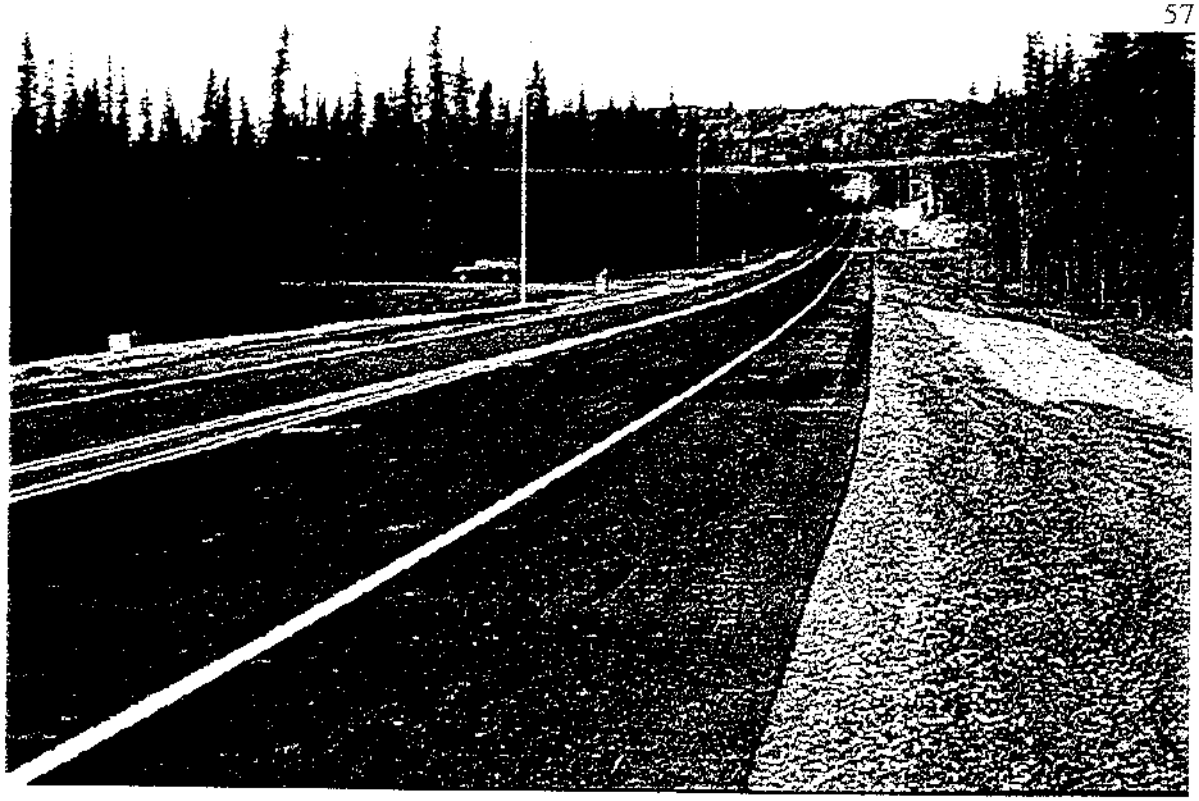

Figure 21. Finished ACE test section.

# 6.0 DATA LOGGING SYSTEM INSTALLATION AND INITIAL DATA COLLECTION

Installation of the data acquisition system began with the placement of the thermistor strings within the ACE test section and in the control section. The locations of these sensor arrays within the test and control sections are shown in Figures 1 and 2. After installation of the arrays was complete, the electrical sub-contractor on the job installed two junction boxes, the traffic highway controller box, and a pedestal-mounted multiplexer enclosure. The wiring from the thermistor strings located at the test section was routed from the side of the embankment into the junction box and then into the base of the traffic controller box. The wiring from the thermistor strings located at the control section was routed to the second junction box and then into the multiplexer enclosure which was located in the ditch adjacent to the control section. The electrical sub-contractor then installed the Campbell Scientific data logging system in the controller box. The instrumentation system is described in detail in the project plans (see reference section) but briefly consisted of a CR10XT data acquisition module which was connected to five AM416 multiplexers and two SM716 memory modules. All equipment with the exception of one multiplexer was located in the traffic controller box adjacent to the test section and is shown in Figure 22. One of the multiplexers was located in the multiplexer enclosure adjacent to the control section. The control section thermistor signals were routed from the multiplexer at the control section through a subsurface wiring harness to the CR10XT data logger located in the traffic controller cabinet. All of the data acquisition hardware was installed by early November of 1996 and actual data collection began on November 16, 1996.

After the first few days of data collection, the data was downloaded from the storage module to a laptop PC and checked for consistency. At that point it was noticed that 5 or 6 of the 192 channels were producing erroneous data. After several work sessions with the instrumentation contractor on hand, we were able to improve the situation, but as of this

writing we still have problems reading several of the channels. Although we have not been able to identify the source of the problem for certain, I believe the difficulty is being caused by contact between one of the thermistor sensor legs and the ground. This is possibly occurring because of a short circuit between the sensor leads and the aluminum shielding rings. This combination produces a galvanic potential on the sensor line since the data logger is grounded through a copper ground rod. The galvanic potential then disturbs the thermistor excitation voltage and causes errors in the recorded signal. This problem was not noticed during the installation of the thermistor strings because the instrumentation contractor used an isolated multimeter for checking the thermistor resistances. At present we are working on a solution to this problem and hope to be able to obtain accurate temperature readings from all sensors by re-wiring those with galvanic potential problems. We are planning on completing the re-wiring before the beginning of the winter '97-'98 season.

Despite the problems discussed above, data acquisition has been ongoing since November of 1996. The data logger is programmed to collect a complete set of temperature data once each hour. It also records ambient air temperature twice each hour and then reports mean daily air temperature, daily minimum temperature, and daily maximum temperature for each 24 hour period.

Figure 23 shows the measured temperature profile within the ACE test section on January 15, 1997 at 12 noon. The figure was generated by fitting temperature contours through the thermistor data using a commercial plotting package. Examination of the figure indicates a convection pattern where low temperature ambient air enters the embankment cross-section at each toe and then travels toward the embankment centerline. Once it reaches the center portion of the embankment, the flow direction gradually becomes vertical and the air exits out the upper surface of the embankment. This flow pattern is responsible for the upward pointed plume which can be observed in Figure 23 near the centerline of the embankment.

Note that flow out of the upper surface of the embankment would normally be prevented by the impermeable asphalt layer. Such was not the case, however, during the '96-'97 winter season, since the embankment had not been paved at that point. We expect to observe a different convection pattern (more similar to the patterns displayed in the calculations discussed in Section 3) during coming winter seasons.

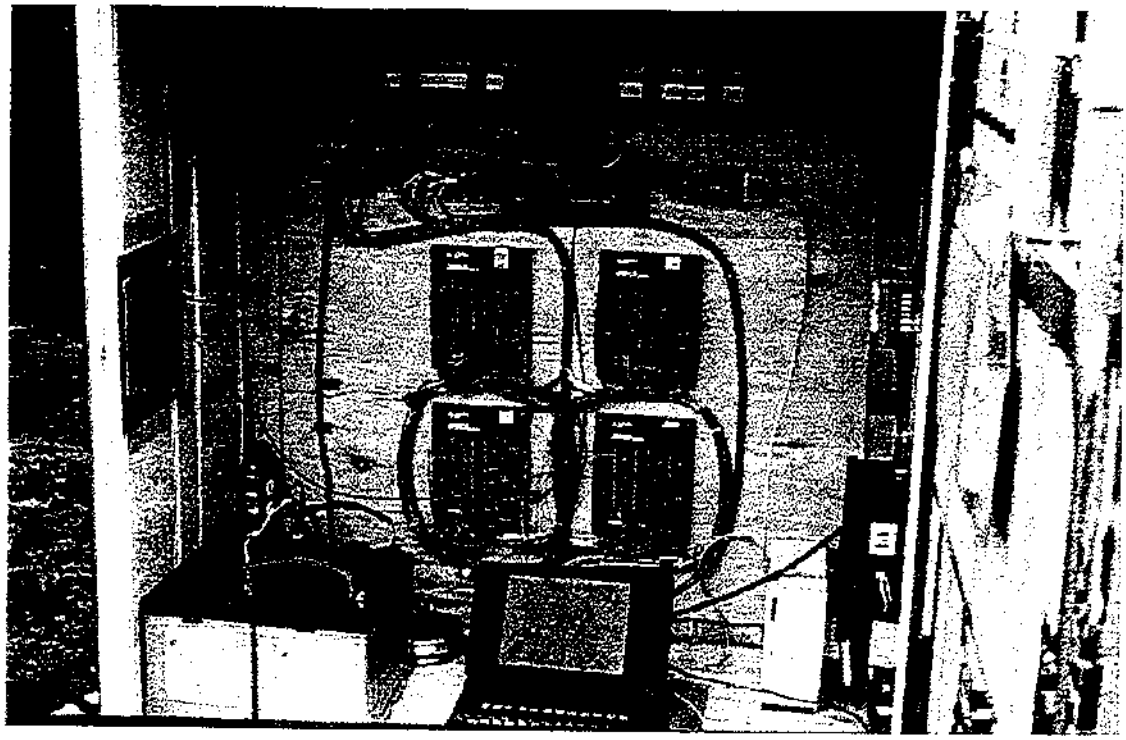

Figure 22. Campbell data logging system installed in highway traffic controller cabinet.

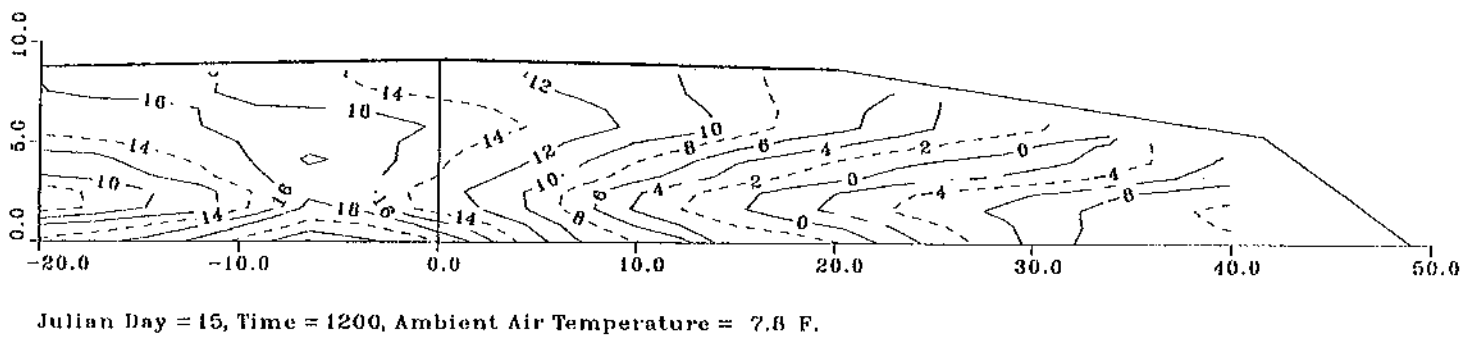


Figure 23. Measured temperature profiles within the test section on January 15, 1997.

# 7.0 CONCLUSIONS

The Phase I portion of this project included a two-year effort to design and build an ACE embankment to be included as an Experimental Feature in Construction in the Parks/Chena Interchange project. This portion of the work has been completed, including the design and construction work for the test section itself and the associated data logging/acquisition system. Problems were encountered with the generation of fines during the placement of the ACE material and approximately 5% of the thermal sensors that were installed did not work properly initially (most of these sensor problems have been corrected via re-wiring as of this writing). Other than these difficulties, the Phase 1 work has been a complete success.

The Phase II portion of the project is on-going at present and will extend at least until 1999. The Phase II work involves systematic data collection and analysis in order to assess the operational characteristics of the ACE test section. It is envisioned that long-term monitoring of the test section will continue beyond the 1999 date.

# 8.0 REFERENCES

Alaska Department of Transportation & Public Facilities, *Parks/Chena Ridge Interchange Project No. NH-I-OA405(7)/63538.* 1996.

Berg, R.L., *Thermoinsulating Media Within Embankments on Perennially Frozen Soil.* Cold Regions Research and Engineering Laboratory Report No. CRREL-SR-76-3, 1976.

Esch, D.C., *Insulation Performance Beneath Roads and Airfields in Alaska.* Transportation Research Record 1146, 1987.

Goering, D.J., and Kumar, P., *Winter-time convection in open-graded embankments.* Cold Regions Science and Technology, Vol. 24, pp. 57-74, 1996.

Goering, D.J., *Air Convection Embankments for Roadway Construction in Permafrost Zones.* Proceedings of the Eighth International Conference on Cold Regions Engineering, Fairbanks, AK, August 1996.

Reckard, M., Esch, D., and McHattie, R., *Peat Used as Roadway Insulation Over Permafrost - Results From the Canyon Creek Site.* Report No. FHWA-AK-RD-88-11, Federal Highway Administration, Washington DC, 1989.

Reckard, M., *White Paint for Highway Thaw Settlement Control. Interim Report.* Report No. FHWA-AK-RD-85-16, Federal Highway Administration, Washington DC, 1985.

Tu, Z., *Effects of an Open Boundary on Winter Time Free Convection in a Porous Roadway Embankment.* M.S. Thesis, Univ. of Alaska Fairbanks, 1996.

Zarling, J.P. and Braley, W.A., *Thaw Stabilization of Roadway Embankments Constructed Over Permafrost.* Report No. FHWA-AK-RD-87-20, Federal Highway Administration, Washington DC, 1986.

Zarling, J.P., Connor, B., and Goering, D.J., *Air Duct Systems for Roadway Stabilization Over Permafrost Areas.* Proceedings of the Fourth International Conference on Permafrost, Fairbanks, AK, July 1983.